

**DESIGN AND ANALYSIS OF SPARSE MIMO ARRAY
AND SPARSE RECOVERY ALGORITHMS FOR
SUPER-RESOLUTION DOA ESTIMATION**

Ruman KAZI

DESIGN AND ANALYSIS OF SPARSE MIMO ARRAY AND SPARSE RECOVERY ALGORITHMS FOR SUPER-RESOLUTION DOA ESTIMATION

by

Ruman KAZI

in partial fulfillment of the requirements for the degree of
Master of Science
in Electrical Engineering
at Delft University of Technology,
to defend publically on 19 August, 2021

Thesis Committee:

| | |
|-----------------------|----------|
| Prof. dr. A. Yarovoy, | TU Delft |
| Dr. Jianping Wang, | TU Delft |
| Dr. Raj Thilak Rajan | TU Delft |
| Dr. Ozgun Paker | NXP |



ACKNOWLEDGEMENTS

Throughout the progress of this thesis, I have received a great deal of support and assistance.

I would first like to express my sincere gratitude to my thesis supervisor, Prof. dr. Alexander Yarovoy. Your expertise in the field of antennas and enthusiasm in the classroom inspired and encouraged me to research in the same field. With your guidance, I was able to formulate my research goals and methodology. Your insightful feedback helped me to stay on the right track.

I would like to thank Dr. Jianping Wang for his guidance through each phase of the thesis. Despite your busy schedule, you were always open to discussion and provided invaluable feedback.

I would also like to thank my supervisors Dr. Ozgun Paker and Ms. Yiting Lu, at NXP Semiconductors. It was not easy to work through these COVID times, but your constant support and weekly meetings helped me achieve the final stage of the thesis. I am immensely grateful that I got to work with you.

I would like to thank the members of my thesis committee, Dr. Alexander Yarovoy, Dr. Jianping Wang, Dr. Raj Rajan and Dr. Ozgun Paker, for taking your time out for assessing my thesis.

The journey for this thesis was not easy. I faced many hurdles, and it was challenging to keep myself motivated due to the COVID restrictions. But the huge encouragement and support from my friends helped me get through tough times. Yvo and Katherine, thank you for your encouragement and faith in me! Thank you, Ameya, for your constant motivation and for being the anchor to keep me sane through these past months.

To my friends, Vijay, Prasad and Divit, I would like to thank you for your pep talks and reassurance to keep my humour alive. And most importantly, a big thank you to my parents for believing in me and providing unconditional support through this journey.

ABSTRACT

The development of Smart Vehicles (SV) has increased the demand for secure and intelligent sensors. The automotive radar plays a massive role in improving the security of these vehicles. Radar needs to make fast and accurate detection in a noisy environment while being aware of its surroundings. The modern radar systems deployed on the SVs utilize multiple sensors to keep track of their surroundings and improve radar cognition. Even though adding more sensors will help make accurate decisions, the processing time to make those decisions may be affected. Hence, the research focuses on improving the accuracy of the decisions without adding extra sensors and extra processing time.

The recent development of the Compressed Sensing (CS) theory has provided new techniques to reduce the number of measurements required for storing the signal and recovering the signal. This idea can be used for Direction-of-Arrival (DOA) Estimation, where we have very few measurements to estimate accurately. Sparse recovery algorithms based on the CS theory have shown promising results for single snapshot DOA estimation. Uniform Linear Array (ULA) provides redundant spatial frequency samples. This redundancy can be reduced by removing specific elements from the array. Removing the redundant elements can help improve the radar's aperture size and angular resolution; these arrays are known as sparse arrays. Combining sparse recovery algorithms with sparse arrays, the angular resolution and accuracy of the DOA estimates can be improved. Based on this idea, an optimal array search algorithm has been proposed in this thesis. The design technique optimizes the Multi-Input-Multi-Output (MIMO) array configuration for improving sparse recovery guarantee. Optimal MIMO topologies, as an example for 2Tx4Rx and 3Tx4Rx (Tx-Transmitters, Rx-Receivers), have been synthesized. The performance of these arrays has been tested with prominent sparse recovery algorithms. The performance of the algorithms is also ranked based on their probability of detection and angular resolution. Improvement in the angular resolution up to 8° with respect to the ULA-MIMO for 2Tx4Rx configuration and up to 5° for 3Tx4Rx configuration is obtained with the help of a sparse recovery algorithm.

CONTENTS

| | |
|--|------------|
| Acknowledgements | v |
| Abstract | vii |
| 1 Introduction | 1 |
| 1.1 Motivation | 2 |
| 1.2 MIMO Radar | 2 |
| 1.3 Sparse Recovery Algorithms | 3 |
| 1.4 Sparse Arrays | 3 |
| 1.5 Problem Statement | 4 |
| 2 MIMO Radar and Signal Model | 5 |
| 2.1 MIMO Radar | 5 |
| 2.1.1 Angle Estimation Basics | 5 |
| 2.1.2 Principle of MIMO Radar | 6 |
| 2.1.3 Multiplexing Strategies | 8 |
| 2.2 MIMO Signal Model | 8 |
| 2.3 Compressive Sensing Theory | 9 |
| 2.3.1 CS Acquisition | 9 |
| 2.3.2 CS Reconstruction | 10 |
| 2.3.3 Necessary and Sufficient Conditions for Perfect Recovery | 10 |
| 2.3.4 Criteria for Optimal Array Topology Search | 11 |
| 2.4 Conclusion | 11 |
| 3 MIMO Array Topology Design | 13 |
| 3.1 Grid-based Optimal Topology Search | 13 |
| 3.2 Grid-less Optimal Topology Search | 14 |
| 3.3 Simulated Annealing | 17 |
| 3.4 Synthesis Results | 20 |
| 3.4.1 Grid-based Optimal Topology search | 20 |
| 3.4.2 Grid-less Optimal Topology search | 21 |
| 3.4.3 Synthesized Array Topology | 21 |
| 3.5 Extensions | 26 |
| 3.5.1 Extension 1 | 26 |
| 3.5.2 Extension 2 | 28 |
| 3.5.3 Extension 3 | 29 |
| 3.6 Conclusion | 30 |

| | | |
|----------|--|-----------|
| 4 | Super Resolution DOA estimation | 31 |
| 4.1 | DOA estimation using sparse recovery | 31 |
| 4.2 | Sparse Recovery Algorithms. | 33 |
| 4.2.1 | Grid-based Algorithms. | 33 |
| 4.2.2 | Greedy Approach | 34 |
| 4.2.3 | Off-Grid Algorithms | 36 |
| 4.2.4 | Gridless Algorithms | 36 |
| 4.3 | Traditional DOA estimation algorithms | 36 |
| 4.3.1 | Deterministic Maximum Likelihood Estimator (DML):. | 37 |
| 4.4 | Performance Analysis | 37 |
| 4.4.1 | Probability of Detection | 38 |
| 4.4.2 | Angular Resolution. | 40 |
| 4.4.3 | Combined Performance | 42 |
| 4.5 | Conclusion | 45 |
| 5 | Conclusion and Future Work | 47 |
| 5.1 | Conclusions. | 47 |
| 5.2 | Future Work. | 48 |
| | References | 49 |

1

INTRODUCTION

The development of radar technology in automobiles has improved the security and decision-making process on roads. The automobile industry uses advanced signal processing algorithms and different techniques to utilize radar technology to suit a specific application and improve its performance. Radar can work efficiently in different weather and light conditions, making it a very appealing choice for sensing purposes.

Research on signal processing algorithms and radar configurations has been evolving more with time. Interesting new aspects are being unfolded these days. However, more improvement on the existing solutions and utilizing new techniques to enhance performance is still open for research.

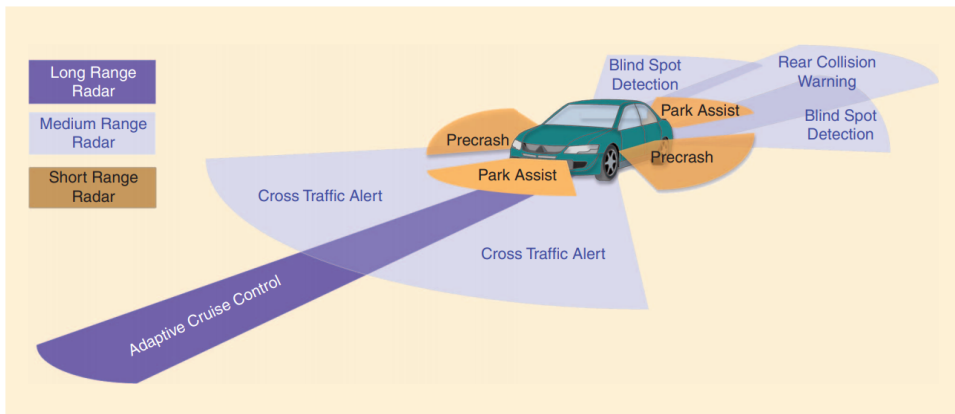


Figure 1.1: Different Ranges of Automotive Radar [1]

1.1. MOTIVATION

Radar is an established sensing technology for Highly Automated Driving (HAD). Radar sensors measure distance, velocity and direction of arrival (DOA) and separate targets into three dimensions. In practice, most targets can be separated in terms of velocity and range as the resolution in these dimensions is much higher than the resolution achievable in the spatial dimension, which is limited by the aperture of the antenna array. However, a high spatial resolution is essential to recognize the objects in the scene better and support advanced HAD applications.

For the cases where the targets lie in the same range-doppler bin, angular signal processing can help discriminate between two closely spaced targets. The angular resolution of an array is dependent on the aperture of the array. A larger aperture will have a higher angular resolution. However, for a larger aperture, more antennas will be required, increasing the resource requirement to recover the signal.

Also, automotive radar needs to make quick and accurate decisions to traverse through a highly dynamic environment on the road. It becomes a high priority to minimize resource requirements without compromising detection accuracy and estimations. Two significant components of the resource requirements are the number of transmitting-receiving channels (number of sensors) and the number of samples required by the signal processing algorithm.

Hence, this project will focus on improving the angular resolution of the array without adding any extra antenna element to the processing chain. We also focus on using a single snapshot algorithm to accurately estimate the targets' location in the angular domain. To achieve our goals, we will also look at the emerging field of Compressive Sensing (CS), which has shown promising results in recovering signals with very few samples. As a result, an optimal array topology coupled with a signal processing algorithm will reduce the resource requirements and achieve the desired accuracy.

1.2. MIMO RADAR

Multi-Input, Multi-Output (MIMO) Radar has been an important topic for research since its inception [2]. Unlike traditional array radars, MIMO radar can transmit orthogonal signals instead of the same scaled signal across all antennas. Although traditional radar has higher processing gain due to a more focused transmitting beam, it would require more time to scan the field of view, making it difficult to use in time-critical and high precision tracking applications.

MIMO radar transmits an omnidirectional signal, illuminating all the angles within the field of view. Multiple transmitters with orthogonal probing signals will illuminate the target, and receiving array will recover from each transmit signal. Since the location of the transmitter array and receiving array is known, the received signals can be phased and combined to form beams in one or more directions (transmitter and receiver beamforming). Hence, MIMO radar is a suitable choice for time-critical, high precision scanning and imaging applications.

A filter bank is used to recover the orthogonal signals at the receiving end. The MIMO radar can be categorized into two categories based on the separation between the transmitting antenna elements. First, MIMO radar with widely spaced antennas[3] where

the antenna elements are widely separated compared to the distance between the target from the radar. As a result, the target RCS (Radar Cross Section) is different for the different transmitters; this helps in better spatial diversity and better detection of the targets. The second, MIMO radar with colocated antennas[4] where the transmitting antennas are closely spaced so that the target RCS remains the same for all. A virtual array can be formed with a larger aperture using the phase difference caused by the different transmitting and receiving antennas.

Using a colocated MIMO, Transmitter(Tx) and receiving(Rx) arrays can form a larger virtual array using fewer antennas. This project will focus on designing such arrays in order to improve the angular resolution of the radar. Thus, from now onwards, the term MIMO radar will be used to reference colocated MIMO Radar.

1.3. SPARSE RECOVERY ALGORITHMS

Compressive Sensing (CS) theory allows compressing a sparse signal into fewer measurements at the time of acquisition[5]. Sparse recovery algorithms faithfully reconstruct the original signal from these fewer measurements (underdetermined problem). These algorithms are *non-adaptive*, i.e., not learning from previous measurements, making them particularly useful for time-critical applications such as Direction-of-Arrival (DOA) estimation in automotive radars. The number of targets is often relatively less than the number of possible angular locations in the field of view, making it a sparse signal in the spatial domain. Hence, one can estimate DOAs using sparse recovery algorithms with a single snapshot.

For a perfect recovery of the signal, there are few necessary and sufficient conditions such as Restricted Isometry Property (RIP)[6, 7] and Mutual Coherence[8]. These properties depend on array topology. Hence, one can design an array to increase the recovery performance of sparse recovery algorithms based on the previous properties.

1.4. SPARSE ARRAYS

Unlike Uniform Linear Arrays (ULA), Sparse Arrays have non-uniform spacing between the elements and have a larger aperture. ULA have uniform spacing between the antennas resulting in high redundancy. Higher resolution can be achieved if the redundant spacing between antennas is reduced, increasing the array's length. A class of linear arrays minimizing this redundancy is called as Minimum-Redundancy Arrays (MRA)[9]. MRA have antenna elements on a uniform grid with missing elements at specific grid points to minimize redundancy. In comparison, sparse arrays can have antennas at any point in the space (gridless). So, MRA can be considered as a subset of sparse arrays.

The concept of MRA can be extended to MIMO configurations as well[10]. Forming an MRA-MIMO provides higher angular resolution compared to traditional radars. Still, MRA-MIMO is bounded by the uniform grid points for antenna locations. Removing this grid constraint can further reduce the redundancy of MRA-MIMO. However, the search for optimal Gridless Sparse-MIMO for large apertures and many antennas becomes highly computationally complex.

Different approaches using genetic and evolutionary algorithms have been used to synthesize optimal non-uniform arrays[11–13]. However, with an increase in the num-

ber of elements and aperture, these techniques' complexity and computational burden increase dramatically. The particle swarm optimization technique is similar to genetic algorithms but computationally less heavy[14]. Deterministic synthesis techniques have also been formulated to solve this problem[15–18]. Even after improving the computational efficiency of these techniques, the analytical complexity remains relatively high.

The use of convex optimization to solve this problem was introduced by H. Lebret et al. in [19]. This method is computationally efficient and an effective alternative technique to design optimal arrays. Based on this, many optimization methods have been proposed, including sparsity-based methods[20, 21], which can take into account mutual coupling[22] and control the minimum spacing between the elements for the physical feasibility of the arrays[23].

The convex optimization approach might lead to local optimum and is sensitive to the initial input points. Thus, simulated annealing is also performed in order to obtain a near-optimum solution.

1.5. PROBLEM STATEMENT

Even with many techniques to synthesize an array, very few have been employed in the MIMO system and none for the Sparse MIMO System. The MIMO virtual array is formed by the combination of Tx and Rx arrays, and in order to obtain an optimal MIMO array, one has to optimize both Tx and Rx arrays.

The project aims to synthesize a Sparse MIMO Topology optimized for maximizing sparse signal recovery guarantee, increase the effective angular resolution of the array, and improve DOA estimation performance using a single snapshot. The work is divided into two sections:

1. Synthesize a realizable optimal Sparse-MIMO Topology
2. Apply sparse recovery algorithms and define performance metrics to be used to select the most suitable algorithm for automotive radar applications

This report is divided into five chapters. Chapter 2 introduces the terminology associated with MIMO Radars and formulates the signal model for future chapters to be used and tested. It also briefs the Compressive Sensing(CS) theory and the necessary conditions for faithful sparse recovery. This condition will help in formulating the optimization problem for synthesizing the sparse MIMO array. Then, the possible extensions of the optimization problem will be discussed. Chapter 4 goes through the prominent sparse recovery algorithms and selects the best candidates for automotive applications. The performance of these algorithms is tested on the synthesized arrays, and comparative analysis is shown. Chapter 5 provides concluding remarks and discusses some potential future work.

2

MIMO RADAR AND SIGNAL MODEL

In this chapter, the radar operation of MIMO is briefly discussed, and the associated signal model is formulated. Followed by a short introduction to Compressive Sensing (CS) theory, the necessary conditions for sparse recovery guarantee are discussed.

2.1. MIMO RADAR

This section introduces the Multiple-Input, Multiple-Output (MIMO) radar and its fundamental principle of operation. MIMO radar refers to radar with multiple TX antennas and multiple RX antennas. MIMO radar provides a cost-effective way to improve the angular resolution of the radar.

2.1.1. ANGLE ESTIMATION BASICS

Estimating the Direction of Arrival (DOA) of a target requires at least two RX antennas. Figure 2.1 shows a radar with one TX and two RX antennas separated by distance ' d '.

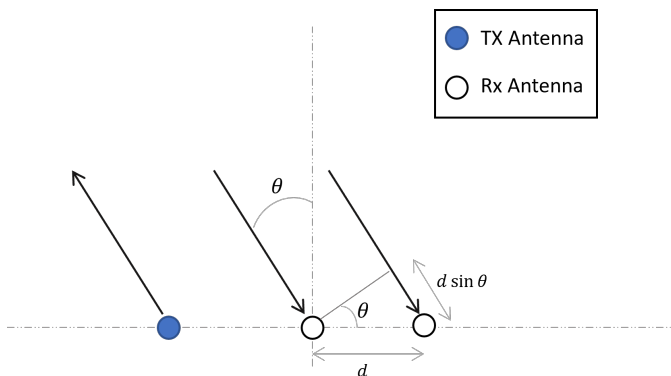


Figure 2.1: Angle Estimation using two RX Antennas

The signal from the TX antenna is reflected from the target (located at angle θ w.r.t. radar) and is received by RX antennas. The signal from the target travels an extra distance of $d \sin(\theta)$ to reach the second RX antenna. Hence, if we calculate this phase difference, we can estimate the direction of arrival of the target using equation 2.1

$$\theta = \sin^{-1}\left(\frac{\omega\lambda}{2\pi d}\right) \quad (2.1)$$

Hence, with more RX antennas, one can receive additional shifts in phase at each antenna. Thus, the phase shifts ω can be reliably estimated by sampling the signal across n RX antennas and performing an FFT (angle-FFT) on this signal sequence. Hence, one can improve angular resolution by adding more antenna elements and increasing the aperture of the effective array.

ANGULAR RESOLUTION:

The resolution of an array with uniformly spaced N antennas is given by the Half-Power Beam Width (HPBW) and is calculated by

$$\Theta_{3dB} = \frac{0.886\lambda}{Nd \sin(\theta_0)} [rad] \quad (2.2)$$

where, d = distance between two elements, θ_0 = desired direction.

For a linear array of N elements, with $d/\lambda = 0.5$

$$\Theta_{3dB}(\theta_0 = 90^\circ) \sim \frac{102^\circ}{N} \quad (2.3)$$

And if we use a sparse array, the aperture is increased, keeping the number of elements the same, reducing HPBW proportionally. A standard MIMO-ULA of 3Tx4Rx configuration provides 12 virtual element ULA arrays. The array resolution at broadside will be given by:

$$\Theta_{3dB}(\theta_0 = 90^\circ) \sim 8.5^\circ \quad (2.4)$$

2.1.2. PRINCIPLE OF MIMO RADAR

Let's take a Single-Input, Multiple-Output (SIMO) radar with 1 TX and 4 RX antennas 2.2. Angle resolution can be doubled by doubling the number of RX antennas as shown in Figure 2.3. Alternatively, using the MIMO concept, the same result can be achieved by adding just one additional TX antenna as shown in Figure 2.4.

This radar has two transmitters TX1 and TX2. A transmitted signal from TX1 will result in a phase shift of $[0 \ \omega \ 2\omega \ 3\omega]$ at the four RX antennas (RX1 is used as a reference). For radar in Figure 2.4, the second TX is placed at $4d$ distance from the first TX, the corresponding signal at receiving end will see an additional phase-shift of 4ω w.r.t transmission of TX1. The phase shift observed at RX antennas due to TX2 will be $[4\omega \ 5\omega \ 6\omega \ 7\omega]$. Combining these phase shifts for four RX antennas, we receive the sequence $[0 \ \omega \ 2\omega \ 3\omega \ 4\omega \ 5\omega \ 6\omega \ 7\omega]$, which is similar to the sequence observed in Figure 2.3. Thus, we can say that the 2TX-4RX antenna configuration can provide a virtual array of 8 antennas.

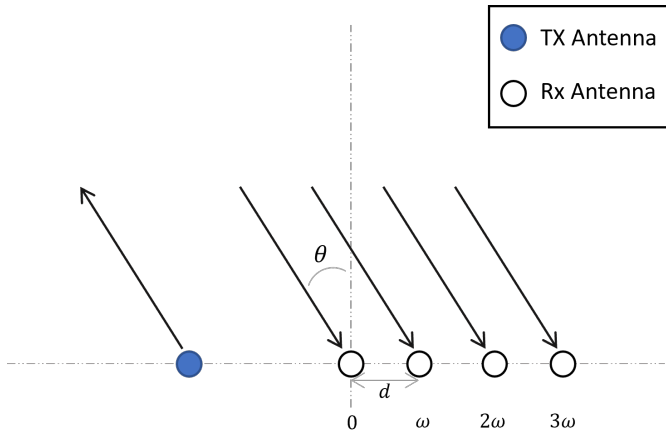


Figure 2.2: Radar with 1 TX and 4 RX antennas

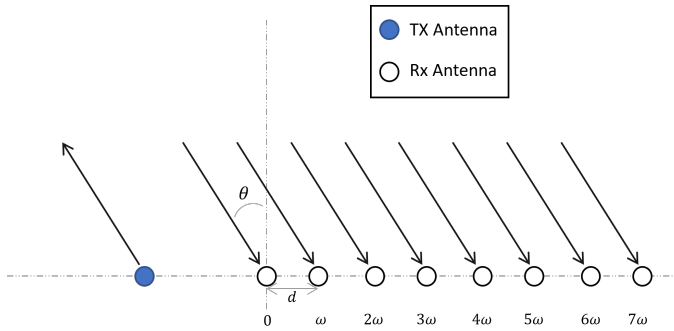


Figure 2.3: Radar with 1TX and 8RX Antennas

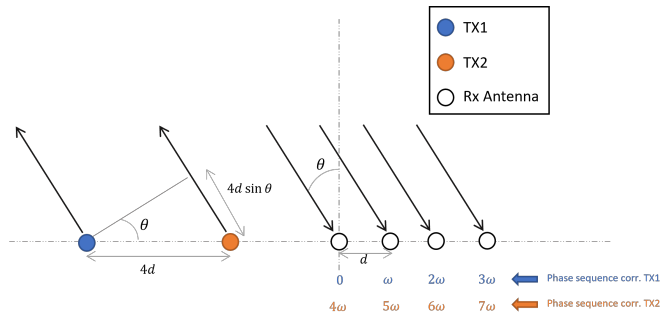


Figure 2.4: Principle of MIMO Radar

To generalize this concept, with nTx (number of TX) and nRx (number of RX) antennas, one can generate a virtual array of $nTx \times nRx$ antennas. Thus, using the MIMO technique, the angular resolution can be improved with fewer additional antennas.

2.1.3. MULTIPLEXING STRATEGIES

The previous section briefed how MIMO radar works using the same RX antennas processing the signal received from multiple TX antennas. Hence, it is essential that the RX antennas can separate the signals corresponding to each TX. There are different ways to achieve this separation of signals. One method is using Time Division Multiplexing (TDM), where the orthogonality is achieved in time. Another method is by sending orthogonal waveforms from each transmitter.

For example, in the automotive application of MIMO radar, Frequency Modulated Continuous Wave (FMCW) signal is used for transmission. Hence, for the TDM method, a chirp signal for a specific duration is assigned to TX1, and the next time slot is assigned to the next TX2. The receiver will assign the received signal in the first time slot to TX1 and the second to TX2.

2.2. MIMO SIGNAL MODEL

If multiple targets lie in the same range bin, the doppler processing can help to distinguish them by determining their velocity. If the range and velocity are also the same for multiple targets, then azimuthal information (angular position) is used to distinguish these targets. We will be focusing on extracting this azimuthal information.

The target is assumed to be in the far-field; thus, we receive planar wavefront at the receive array. As we discussed earlier in Figure 2.4, the direction of arrival creates a path difference between two subsequent receiving antennas. The phase shift caused by this path difference at each antenna can be calculated by:

$$a(\theta_{i,k}) = e^{j\omega_{i,k}} = e^{j\frac{-2\pi}{\lambda}d_i \sin(\theta_k)} \quad (2.5)$$

where $\omega_{i,k}$ is the phase shift caused by k^{th} target at i^{th} receiver, θ_k is the direction of arrival for k^{th} target, λ is the operating wavelength of radar and d_i is the distance between first (reference) antenna and i^{th} antenna.

Hence, the steering vector for TX array:

$$\mathbf{a}_T(\theta_k) = [1, a(\theta_{1,k}) \cdots a(\theta_{nTx,k})]^T \quad (2.6)$$

The steering vector for RX array:

$$\mathbf{a}_R(\theta_k) = [1, a(\theta_{1,k}) \cdots a(\theta_{nRx,k})]^T \quad (2.7)$$

Collecting the reflected signal from K targets over time samples, we obtain

$$\mathbf{y}(t) = \sum_{k=1}^K \gamma_k (\mathbf{a}_T(\theta_k) \otimes \mathbf{a}_R(\theta_k)) s(t - \tau_k) + w(t) \quad (2.8)$$

Where γ_k is the complex scattering coefficient of target k , proportional to its RCS. The term $\mathbf{a}_T(\theta_k) \otimes \mathbf{a}_R(\theta_k)$ can be considered as the steering vector of the virtual array for k^{th} target at direction of arrival at θ_k . $s(t)$ is the reflected signal, τ_k is the delay caused by the range of the target from radar. And $w(t)$ is assumed to be White Gaussian Noise. The

complex scattering coefficients for all the targets is assumed to be uniform and equal to 1 for the automotive radar case. Using virtual array steering vector:

$$\mathbf{a}(\theta_{\mathbf{k}}) = \mathbf{a}_T(\theta_{\mathbf{k}}) \otimes \mathbf{a}_R(\theta_{\mathbf{k}}) = [1, a(\theta_{1,k}) \cdots a(\theta_{nTx-nRx,k})]^T \quad (2.9)$$

After discretization, the signal model becomes:

$$\mathbf{y} = \mathbf{A}\mathbf{s} + \mathbf{W} \quad (2.10)$$

where,

$$\mathbf{A} = [\mathbf{a}(\theta_1), \mathbf{a}(\theta_2), \cdots, \mathbf{a}(\theta_K)] \quad (2.11)$$

$$\mathbf{S} = [s_{\tau_1} \cdots s_{\tau_K}]^T, \text{ where } \mathbf{s}_{\tau_k} = [s(-\tau_k), s(1-\tau_k), \cdots, s(N-\tau_k)] \quad (2.12)$$

Where N = number of snapshots, and \mathbf{W} contains complex Gaussian White noise.

This signal model will be used in the following chapters for testing the performance of the synthesized arrays and algorithms.

2.3. COMPRESSIVE SENSING THEORY

After the famous Shannon sampling theorem, the introduction of Compressive Sensing (CS) theory has been a breakthrough for Signal Processing Field. CS theory is useful for the acquisition of signals which are compressible or sparse. CS can overcome the sampling rate Nyquist-criterion and use fewer samples to represent the signal. And using some non-linear reconstruction techniques, the signal can be recovered with sufficient guarantee from fewer measurements. Now, we will look at the essential concepts underlying CS:

2.3.1. CS ACQUISITION

Let $\mathbf{s} \in \mathbb{R}^n$ be the signal vector to be recovered. The compressive sensing theory (CS) suggests that, one can define a measurement matrix \mathbf{A} that 'compresses' signal \mathbf{s} into a smaller dimension vector $\mathbf{y} \in \mathbb{R}^m$ where $m < n$. And, still be able to recover the signal \mathbf{s} from the measurement vector \mathbf{y} with sufficient guarantee but only if the signal \mathbf{s} is a 'Sparse Signal.' Since, \mathbf{A} has fewer rows than columns, it becomes an underdetermined system (refer Figure 2.5) which implies that for specific signal \mathbf{s}_0 there is no unique solution such that for $\mathbf{y} = \mathbf{A}\mathbf{s} = \mathbf{A}\mathbf{s}_0 \Rightarrow \mathbf{s} \neq \mathbf{s}_0$. Hence to enable faithful recovery, this theory limits to special input signals \mathbf{s} : Sparse Signals.

Sparsity is an important parameter in CS theory, which implies that signal \mathbf{s} has only very few non-zero values. Mathematically, this can be expressed as $\|\mathbf{s}\|_0 \leq k$ where $\|\cdot\|_0$ denotes l_0 -norm, which counts the number of non-zero values. A signal \mathbf{s} is called sparse signal if $k \ll n$. The exhaustive search can be done to recover sparse signal \mathbf{s} from the measurements \mathbf{Y} but it becomes NP-Hard problem to solve. One of the options is to use l_1 -norm as given by equation 2.13.

$$\hat{\mathbf{s}} = \arg \min_{\mathbf{s}} \|\mathbf{s}\|_1 \quad \text{s.t. } \mathbf{A}\mathbf{s} = \mathbf{y} \quad (2.13)$$

$\|\mathbf{s}\|_1$ denotes the l_1 -norm of signal \mathbf{s} , which represents the absolute sum of the elements of a vector.

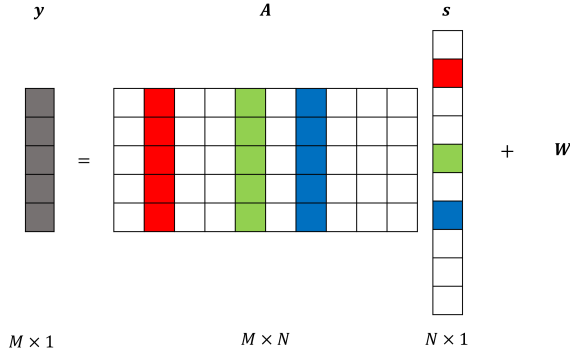


Figure 2.5: Undetermined System for Sparse Signal 's'

2.3.2. CS RECONSTRUCTION

Let the number of targets in the radar field of view to be k . If we select a uniform grid of scanning angles for DOA estimation consisting of n points on grid such that $k \ll n$, then we have *sparsity* (number of targets) in spatial domain. The respective steering matrix formed by the uniform scanning grid will have dimensions of $m \times n$ where m = number of receiving elements.

$$\mathbf{A} = \begin{bmatrix} 1 & 1 & \cdots & 1 \\ a(\theta_{1,1}) & a(\theta_{1,2}) & \cdots & a(\theta_{1,n}) \\ a(\theta_{2,1}) & a(\theta_{2,2}) & \cdots & a(\theta_{2,n}) \\ \cdots & \cdots & \cdots & \cdots \\ a(\theta_{m-1,1}) & a(\theta_{m-1,2}) & \cdots & a(\theta_{m-1,n}) \end{bmatrix} \quad (2.14)$$

And the signal \mathbf{s} vector will have non-zero values at k locations. If we define, support of $\mathbf{s} = \text{supp}(\mathbf{s})$ = set of indices over which \mathbf{s} is non-zero. Let \mathbf{s}_s be the vector \mathbf{s} restricted to its support and similarly, \mathbf{A}_s denotes the columns of \mathbf{A} corresponding to that support. This support will correspond to the respective DOA for the targets i.e. \mathbf{A}_s will be the set of columns corresponding to the array response vectors of the DOA of targets. So we have $\mathbf{y} = \mathbf{A}\mathbf{s} = \mathbf{A}_s\mathbf{s}_s$. When the support is known, we can recover \mathbf{s} from \mathbf{y} via $\mathbf{s}_s = (\mathbf{A}_s^T\mathbf{A}_s)^{-1}\mathbf{A}_s^T\mathbf{y}$ assuming that \mathbf{A}_s has full column rank. Hence, the task of sparse recovery algorithms is to determine this support. Once we know the support of 's', then we can determine the non-zero locations and recover the original signal.

2.3.3. NECESSARY AND SUFFICIENT CONDITIONS FOR PERFECT RECOVERY

The ability to recover signal \mathbf{s} from measurements $\mathbf{y} = \mathbf{A}\mathbf{s}$ depends on the properties of CS matrix \mathbf{A} . In most general case where CS theory used is in Underdetermined Problems. So, there can be infinite solution possible. The CS theory aims to find the sparsest solution to the problem. Thus, it is important to determine conditions on \mathbf{A} to ensure recovery.

RESTRICTED ISOMETRY PROPERTY (RIP)

Necessary condition for recovering signal vector - \mathbf{s} from the measurement of \mathbf{y} is that the matrix \mathbf{A} must obey RIP of order k , as given in equation 2.15.

$$(1 - \delta) \|\mathbf{s}\|_2^2 \leq \|\mathbf{A}\mathbf{s}\|_2^2 \leq (1 + \delta) \|\mathbf{s}\|_2^2. \quad (2.15)$$

and $\delta > 0$ is known as restricted isometry constant. This condition states that the matrix \mathbf{A} must preserve the distance between two k -sparse vectors. It has been found in the literature that calculating the value of δ itself is very hard, so another simpler popular condition which guarantees stable recovery is Mutual Coherence.

MUTUAL COHERENCE

Mutual Coherence of a dictionary \mathbf{A} , denoted by $\mu(\mathbf{A})$ [24] is the maximum absolute cross-correlation of its columns:

$$\mu(\mathbf{A}) = \max_{1 \leq i \neq j \leq n} \frac{|a_i^H a_j|}{\|a_i\|_2 \|a_j\|_2}, \quad (2.16)$$

where, a_i is the i^{th} column of \mathbf{A} .

Lower value of $\mu(\mathbf{A})$ is desired for higher recovery guarantee.

2.3.4. CRITERIA FOR OPTIMAL ARRAY TOPOLOGY SEARCH

Even though **RIP** provides robust recovery guarantee, it is difficult to calculate. *Mutual Coherence* (MC) - $\mu(\mathbf{A})$ has been shown to provide acceptable recovery guarantee and most efficient to compute [25]. It is clear that we want to *reduce* the value of $\mu(\mathbf{A})$ as much as possible to improve recovery guarantee.

The equation 2.16 states that $\mu(\mathbf{A})$ depends on the array topology (the rows of \mathbf{a}). Hence we can search for an array topology which can minimize this value. Hence, our goal for optimization problem for search of optimal array will be minimizing $\mu(\mathbf{A})$.

2.4. CONCLUSION

In this chapter, the MIMO radar concept and its effect on improving the angular resolution of the radar are analyzed. The virtual array for MIMO from the transmitter and receiver array is created by transmitting orthogonal waveforms. The receiving array receives the waveform and is associated with the transmitting element that transmitted that waveform.

The Compressive Sensing theory requires fewer measurements to recover a sparse signal. Since the number of targets will always be \ll the possible angular locations in the Field-of-View of radar, the DOA estimation problem can be formulated as a sparse recovery problem. Sparse recovery guarantee can be improved with the low mutual coherence of the measurement matrix. For the DOA signal model, the steering matrix is the measurement matrix. Hence, the goal problem can be formulated by finding the steering matrix with the lowest mutual coherence to ensure maximum recovery.

3

MIMO ARRAY TOPOLOGY DESIGN

Recently, sparse array topologies synthesized from Non-Uniform Spaced Linear Arrays (NSULA) have been introduced in order to improve the effective aperture of the array and reduce spatial redundancy [13], [9]. This chapter describes two techniques for designing a non-uniformly spaced Sparse MIMO antenna topology to improve radar performance. The goal will be to obtain a non-uniformly spaced transmitter and receiver array topology creating a virtual array with a larger aperture and lowest mutual coherence value.

3.1. GRID-BASED OPTIMAL TOPOLOGY SEARCH

Similar to thinning strategy[26], a sequence of antennas are turned on or off from a set of possible antenna locations. The transmitter and receiver antenna arrays will combine and form the virtual array of desired aperture $L\lambda/2$ units. The steps to obtain a grid-based optimal array are as follows:

STEP 1

Define a Uniform Linear Array Antenna having L elements with $\lambda/2$ unit spacing. The number of transmitters and receivers in the desired MIMO is n_{Tx} and n_{Rx} , respectively.

STEP 2

1. The possible transmitter and receiver arrays will lie within the larger L element ULA
2. The first antenna of the receiver array and transmitter array is taken as reference location with zero distance. $d_{i,R}$ is the location of i^{th} receiver in terms of $\lambda/2$ units from the reference. Similarly, $d_{j,T}$ is the location j^{th} transmitter.
3. The position of the last element, the receiver array, and the transmitter array's last element have the constraint to attain the desired aperture.

$$d_{n_{Rx},R} + d_{n_{Tx},T} = L \quad s.t. \quad d_{n_{Rx},R} < d_{n_{Tx},T} \quad (3.1)$$

where, $d_{nRx,R}$ and $d_{nTx,T}$ are the distance of the last element of receiver array and transmitter array from the reference respectively. The possible configurations

4. Similarly,

$$d_{i,R} < d_{i+1,R} < d_{j,T} < d_{j+1,T} \quad (3.2)$$

5. Following the above constraints, the possible transmitter and receiver arrays are stored in H_T and H_R , respectively.

6. All the possible virtual arrays formed from the sets H_T and H_R are stored in H

STEP 3

1. Select a angular grid for creating steering matrix \mathbf{A} . For example, A grid for angles -90° to 90° with step size of 1 degrees(181 grid points).
2. Using virtual arrays from the set of H , steering vector a can be generated for each scan angle and thus the steering matrix \mathbf{A}

$$\mathbf{A} = [a(\theta_1), a(\theta_2), \dots, a(\theta_p)] \quad (3.3)$$

STEP 4

1. As defined in the previous chapter, the goal is obtain the configuration that leads to the lowest Mutual Coherence $\mu(\mathbf{A})$.

$$\mu(\mathbf{A}) = \max_{1 \leq i \neq j \leq n} \frac{|a_i^H a_j|}{\|a_i\|_2 \|a_j\|_2}, \quad (3.4)$$

where a_i is the i^{th} column of steering matrix \mathbf{A} .

2. For each virtual array from the set H , generates the steering matrix \mathbf{A} and the $\mu(\mathbf{A})$ is calculated.
3. The virtual array that results in the lowest $\mu(\mathbf{A})$ value is selected, and respective transmitter and receiver arrays that formed that array is selected as the grid-based optimal arrays,

The transmitter and receiver arrays obtained from this search will be used for testing the performance of DOA estimation against the results of grid-less optimal array search.

3.2. GRID-LESS OPTIMAL TOPOLOGY SEARCH

In the literature on antenna array topology optimization, being motivated by the practicality and optimum power efficiency of uniformly excited arrays [27], many uniform amplitude array synthesis techniques have been proposed [11, 16, 28–30]. It is also important to ensure minimum inter-element spacing to avoid thermal problems, high mutual coupling levels and unrealizable design.

Characteristics of state-of-art methods for optimum antenna array topology synthesis have been compared against the superior proposed method in [31]. The proposed

method in [31] applies more advanced optimization constraints than any previously published articles. However, the method has not been developed for Sparse MIMO arrays. This chapter will extend this method for Sparse MIMO arrays and obtain optimum Transmitter and Receiver Array Topology for the desired aperture.

Let us consider an nTx and nRx element uniformly excited linear transmitter and receiver array, respectively. The steering vectors formed by the transmitting and receiving array can be given by:

$$\mathbf{a}_T(\theta_p) = [a_{T,0}(\theta_p), a_{T,1}(\theta_p) \cdots a_{T,nTx}(\theta_p)] \quad (3.5)$$

$$\mathbf{a}_R(\theta_p) = [a_{R,0}(\theta_p), a_{R,1}(\theta_p) \cdots a_{R,nRx}(\theta_p)] \quad (3.6)$$

with,

$$a_{T,n}(\theta_p) = e^{jkx_n \sin(\theta_p)}, \quad a_{R,m}(\theta_p) = e^{jky_m \sin(\theta_p)} \quad (3.7)$$

where, θ_p is the angular position of the p^{th} target, x_n and y_m are the positions of the n^{th} transmitter and m^{th} receiver respectively. And $k = \frac{2\pi}{\lambda}$. Using the Kronecker Product of these vectors ($\mathbf{a}(\theta_k) = \mathbf{a}_T(\theta_k) \otimes \mathbf{a}_R(\theta_k)$) we obtain steering vector of the virtual array formed as

$$\mathbf{a}(\theta_p) = [a_0(\theta_p), a_1(\theta_p) \cdots a_{nRx \cdot nTx}(\theta_p)]^T \quad (3.8)$$

where

$$a_{m+n}(\theta_p) = e^{jk(x_n + y_m) \sin(\theta_p)} \quad (3.9)$$

Using the iterative method proposed in [28], we start with a transmitter linear array with spacing ($nRx \cdot d_{ini}$) and receiver linear array with spacing d_{ini} . And move n^{th} transmitter element by ϵ^i , m^{th} receiver element by δ^i at the i^{th} iteration. The new position of the elements will be:

$$x_n^i = x_n^{i-1} + \epsilon_n^i, \quad y_m^i = y_m^{i-1} + \delta_m^i \quad (3.10)$$

Substituting (3.10) in (3.9), the expression for steering vector becomes:

$$a_{m+n}(\theta_p) = e^{jk(x_n^{i-1} + \epsilon_n^i + y_m^{i-1} + \delta_m^i) \sin(\theta_p)} \quad (3.11)$$

As realized in [28], the far-field expression in (3.11) can be linearized around the element positions using the Taylor expansion when following relations hold:

$$\left| \frac{2\pi}{\lambda} \sin\theta (\epsilon_n, \delta_m)^i \right| \ll 1, \quad i.e. \quad |(\epsilon_n, \delta_m)^i| \ll \lambda/2\pi = 0.16\lambda \quad (3.12)$$

If sufficiently small high-order terms ignored to keep the convexity of the problem, the approximated expression at i^{th} iteration:

$$a_{m+n}(\theta_p) \approx e^{jk(x_n^{i-1} + y_m^{i-1} + \delta_m^i) \sin(\theta_p)} \times (1 + jk\epsilon_n^i \sin(\theta_k) + jk\delta_m^i \sin(\theta_k)) \quad (3.13)$$

This approximated expression will be used to formulate the new steering vector. The subsequent new steering matrix:

$$\mathbf{A} = [\mathbf{a}(\theta_1), \mathbf{a}(\theta_2) \cdots \mathbf{a}(\theta_p)] \quad (3.14)$$

For the compressed sensing terminology, we will call the columns of steering matrix \mathbf{A} as atoms. Assume that we have P atoms in \mathbf{A} . In order to calculate the mutual coherence amongst the columns, we will define a function f and using equations 3.13 and 3.14,

$$f_{\epsilon_n, \delta_m}^i(\theta_s) \approx \max_{a \neq b} \sum_{n=1}^{nTx} \sum_{m=1}^{nRx} e^{jkx_n^{i-1}(\sin\theta_a - \sin\theta_b)} \times e^{jky_m^{i-1}(\sin\theta_a - \sin\theta_b)} \\ \times (1 + jk\epsilon_n^i(\sin\theta_a - \sin\theta_b) + jk\delta_m^i(\sin\theta_a - \sin\theta_b)) \dots \quad \{\theta_a, \theta_b \in \theta_s\} \quad (3.15)$$

Where the input to the function $f(\theta_s)$, is the set of angles from the selected Field-of-View. The vectors of parameters for the i^{th} iteration are given by:

$$\mathbf{x}^i = [x_1^i, x_2^i, \dots, x_{nTx}^i]^T \quad \mathbf{y}^i = [y_1^i, y_2^i, \dots, y_{nRx}^i]^T \quad (3.16)$$

$$\boldsymbol{\epsilon}^i = [\epsilon_1^i, \epsilon_2^i, \dots, \epsilon_{nTx}^i]^T \quad \boldsymbol{\delta}^i = [\delta_1^i, \delta_2^i, \dots, \delta_{nRx}^i]^T \quad (3.17)$$

The set of p angles for θ_s forms the following vector:

$$\theta_s = [\theta_1, \theta_2, \dots, \theta_p] \quad (3.18)$$

To calculate inter-element spacing at each iteration a $(nTx \cdot nRx - 1) \times nTx \cdot nRx$ circulant matrix D is formed.

$$D = \begin{bmatrix} -1 & 1 & 0 & 0 & \dots & \dots & 0 \\ 0 & -1 & 1 & 0 & \dots & \dots & 0 \\ 0 & 0 & -1 & 1 & \dots & \dots & 0 \\ 0 & \ddots & \ddots & \ddots & \dots & \dots & \vdots \\ \vdots & \ddots & \ddots & \dots & -1 & 1 & 0 \\ 0 & \dots & \dots & \dots & 0 & -1 & 1 \end{bmatrix} \quad (3.19)$$

An additional condition is imposed in order to set the first element positions of transmitter array and receiver array is same as required by the MIMO Linear Array setup. It is given by:

$$\epsilon_1^i = \delta_1^i \quad (3.20)$$

Finally, if the limit of aperture size is set, an additional condition should be forced on the element positions at each iteration so that the effective aperture is equal to the set limit on aperture. This condition is given as:

$$|(x_{nTx}^{i-1} + \epsilon_{nTx}^i + y_{nRx}^{i-1} + \delta_{nRx}^i) - (x_1^{i-1} + \epsilon_1^i + y_1^{i-1} + \delta_1^i)| = L \quad (3.21)$$

Using far-field equation (3.11) and the above-defined vectors for parameters, we can formulate an iteration based convex optimization problem. At each iteration the following convex optimization problem will be solved:

$$\begin{aligned}
& \underset{\epsilon^i, \delta^i}{\operatorname{argmin}} \mu \\
& \text{s.t. } \max |f_{\epsilon_n, \delta_m}^i(\theta_s)| < \mu \\
& |\epsilon^i| \leq \beta, |\delta^i| \leq \beta, \epsilon_1^i = \delta_1^i \\
& D * ((\mathbf{x}^{i-1} + \epsilon^i) \otimes (\mathbf{y}^{i-1} + \delta^i)) \geq d_{min} \\
& |(x_{nTx}^{i-1} + \epsilon_{nTx}^i + y_{nRx}^{i-1} + \delta_{nRx}^i) - (x_1^{i-1} + \epsilon_1^i + y_1^{i-1} + \delta_1^i)| = L
\end{aligned} \tag{3.22}$$

μ is the maximum Mutual Coherence amongst the columns of steering matrix, which is simultaneously minimized for all the defined angles within Field-of-View (FOV) θ_s . $|\epsilon^i|$ & $|\delta^i|$ are upper bounded by user-defined constant β as followed by equation (3.12). Setting $\epsilon_1^i = \delta_1^i$ ensures the first element of transmitter and receiver are equally shifted. The last two constraints guarantee that the minimum inter-element spacing at each iteration is larger than or equal to the desired value, d_{min} and the desired aperture size is defined as L .

The optimization problem presented in (3.22) is a non-linear convex problem, namely a second-order cone program [32], which can efficiently solved using interior-point methods by available solvers such as CVX [33]. In this thesis, an off-the-shelf CVX solver will be used to synthesize the non-uniform Sparse MIMO configuration. The optimization problem 3.22 provides the transmitter and receiver array optimized for minimizing Mutual Coherence for predefined Field-of-View (FOV).

3.3. SIMULATED ANNEALING

Using the convex optimization technique, we can not solve all the synthesis problems; only local optima are found, and the choice of the initial point is also very crucial [19]. Thus, the algorithm can get stuck at local optima. In order to get out of these local optima points, there are various Metaheuristic techniques available in the literature, such as Hill Climbing and Simulated Annealing. Hill climbing is a relatively simple algorithm but has a higher chance of getting stuck at another local optimum.

The Simulated Annealing (SA) approach introduced in [34] comes from the 'annealing' technique in metallurgy, which involves heating and cooling of a material to reduce the defects. The heating adds randomness (energy) to the system, and cooling will lead to a more stable configuration of the crystals. This approach can be adapted to the optimization problems stuck at local optimums. Hence, Simulated Annealing applies to only specific optimization problems that utilize this technique. This technique does not guarantee a global optimum solution but approximates a global-optimum solution if the appropriate temperature curve is selected.

For all the possible initial input antenna topologies (set of H) to the optimization problem 3.22, the obtained mutual coherence μ may follow the curve in Figure 3.1. The figure tells us that the optimization problem can get stuck at local optima when the initial input Topology is $T1 \in H$.

Let us assume that for a specific configuration of MIMO, the optimization problem is stuck at local optima when initial input topology $T1$ was used. So it is possible that a

global optima solution can be obtained if the initial input to the optimization problem was different (e.g. if it started with T3 topology).

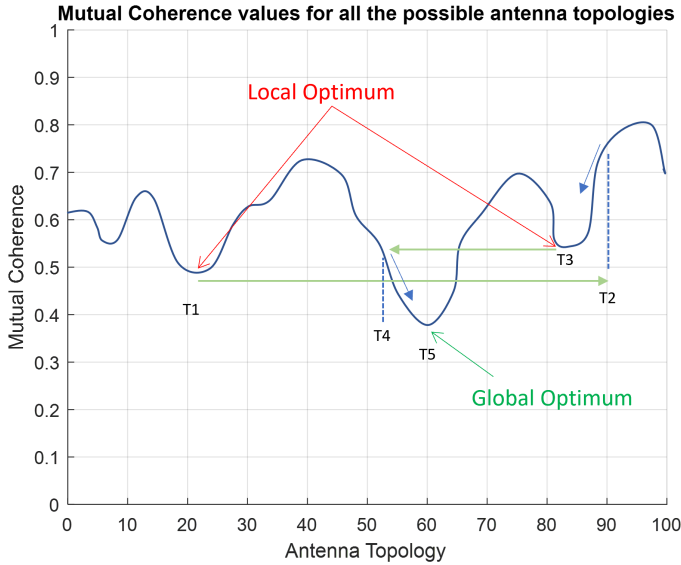


Figure 3.1: Simulated Annealing Technique

Steps involved in the simulated annealing approach:

1. The temperature curve defined in Figure 3.2 provides the amplitude for a random shift in the topology to be selected for the next iteration. Hence, a more significant shift in the topology (e.g. T2) is observed with a high temperature at the beginning.
2. Using this new topology as input to the optimization problem 3.22, a new solution is obtained that may or may not be stuck at the local optimum. At this point, the temperature-dependent acceptance curve 3.3 helps in accepting worse solutions. So if the temperature is high, a high level of acceptance for a worse solution is tolerated, and the algorithm settles towards that point. Even if the next local optima (T3) is worse than the previous optima, the simulated annealing method helps get out of the local optima point.
3. Then, for the next iteration, the topology is shifted depending on the temperature at that point. As the temperature has cooled down for the next iteration, the shift in the amplitude should be smaller than the previous iteration. And this new topology (e.g. T4) is used as the initial point for the optimization problem.
4. This process is repeated until the temperature reaches zero or the optimization provides a worse solution than the acceptable value at that temperature.
5. The algorithm should converge towards global-optimum solution.

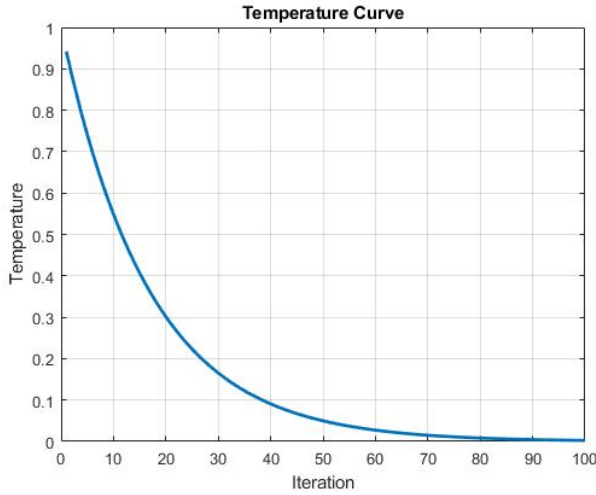


Figure 3.2: Temperature curve for shifting the topology.

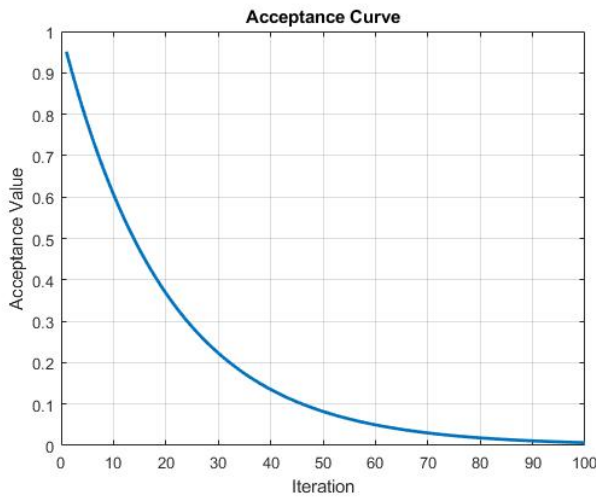


Figure 3.3: The acceptance curve

As we can notice, Simulated Annealing approach helps in getting out of local optima points and provides chance to move towards global optima solution. It is important to note that this process is very sensitive to the nature of temperature and acceptance curves. A balanced curve will provide the best chance to reach global optimum solution. Overall, simulated annealing will help us in reaching better solutions.

3.4. SYNTHESIS RESULTS

In this section, we will look at the synthesized arrays resulting from the previously defined optimization algorithms. We will compare the results from the grid-based optimal array search against the grid-less optimal array search. In automotive applications, 2Tx4Rx and 3Tx4Rx MIMO radar configurations are most commonly used. Hence, our search algorithm will focus on these two configurations. The modern radars operate in the range of 76-78GHz. Thus we will select 77GHz as the operating frequency for our synthesis.

Based on the application, the automotive radars are designed to work in the Short Range, Mid Range and Long Range. A wider Field-of-View for radar's operation is required for short-range, while a very short Field-of-View is scanned for long-range radar. Depending on the various applications in the automotive industry, we can divide the Field-of-View for different ranges of operation of radars, summarized in table 3.1:

| FOV (degrees) | Range |
|---------------|--------------|
| [-15 to 15] | Long Range |
| [-30 to 30] | Medium Range |
| [-50 to 50] | Short Range |

Table 3.1: The Field-of-View (FOV) of the radar for different range of operation

The setup for testing the algorithms for both configuration:

2Tx4Rx - MIMO CONFIGURATION

$n_{Tx} = 2$, $n_{Rx} = 4$ with minimum inter-element spacing $d_{min} = 0.5\lambda$, we will set the desired aperture size $L = 19\lambda/2$. The reason for defining this aperture size is because it is used in industry-standard MRA-MIMO for 2Tx4Rx.

3Tx4Rx - MIMO CONFIGURATION

$n_{Tx} = 3$, $n_{Rx} = 4$ with minimum inter-element spacing $d_{min} = 0.5\lambda$. Since, a standard Uniform Linear MIMO Array with 3Tx4Rx has aperture size of $11\lambda/2$. We will set the desired aperture size $L = 22\lambda/2$ in order to double the angular resolution of the synthesized array.

3.4.1. GRID-BASED OPTIMAL TOPOLOGY SEARCH

The algorithm looks for the virtual array with the lowest mutual coherence (μ) value by performing the exhaustive search for the possible MIMO configurations with given constraints. The antennas are assumed to lie on a uniform grid with $\lambda/2$ spacing. The respective transmitting and receiving arrays are selected as the grid-based optimal arrays.

It has been observed that the grid-based optimal array search algorithm results lead towards Restricted - Minimum Redundancy MIMO Array for the given apertures. Hence, the results of this search will be called MRA-MIMO results from now onward. It is also important to note that the search algorithm remains independent of Field-of-View(FOV) selection. Hence the resulting arrays have the same performance for any FOV.

3.4.2. GRID-LESS OPTIMAL TOPOLOGY SEARCH

The iterative optimization problem 3.22 requires a initial MIMO configuration to start the algorithm. The result obtained from the grid-based search is taken as the starting point for the algorithm. The maximum shift (β) is set to $= 0.16\lambda$. The algorithm is tested for different Field-of-Views (FOV). The algorithm provides us with the transmitter (TX) and receiver (RX) array directly as the output while minimizing the mutual coherence value μ . This algorithm does not have the grid constraint for the physical location of the antennas. Hence, the synthesized arrays from this algorithm can take any position in the space, providing more freedom to the algorithm to look for optimum array positions.

There is a chance of the optimization algorithm getting stuck at local optima, and thus the simulated annealing has been performed to get the optimization out of local optima. As discussed earlier, the simulated annealing method was implemented for both the configurations and the results after the simulated annealing are summarized in the following section.

3.4.3. SYNTHESIZED ARRAY TOPOLOGY

The result of the both algorithms are presented in this section. The algorithms provide transmitting array (TX), receiving array (RX) and the virtual array with lowest possible mutual coherence (μ) for given FOV and aperture size.

2Tx4Rx - MIMO

The synthesis result from the both optimization algorithms are summarized in the following tables (Table 3.2 and 3.3).

| Position of TX and RX arrays ($\lambda/2$ units) | | | | | | |
|---|----|---------|----|--------|--------|---------|
| FOV | TX | | RX | | | |
| | 1 | 2 | 1 | 2 | 3 | 4 |
| [-15 to 15] | 0 | 10.3022 | 0 | 2.4794 | 5.3829 | 8.6977 |
| [-30 to 30] | 0 | 11.1357 | 0 | 1.8041 | 3.2855 | 7.8642 |
| [-50 to 50] | 0 | 12.8436 | 0 | 1.0165 | 4.0965 | 6.15630 |
| MRA | 0 | 13 | 0 | 1 | 4 | 6 |

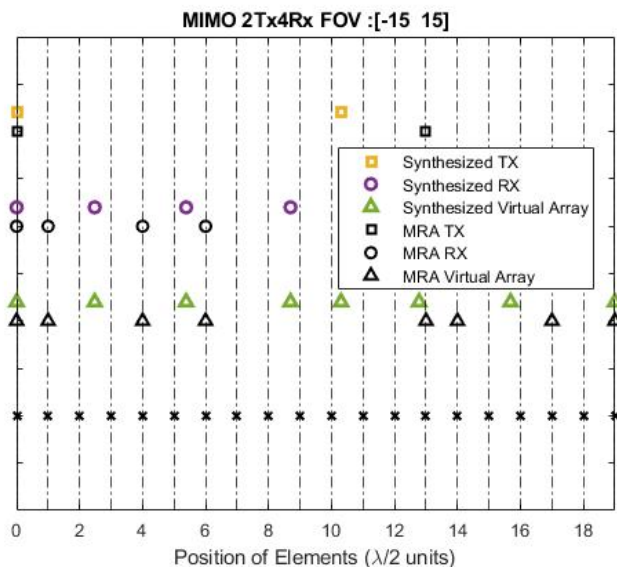
Table 3.2: TX and RX positions obtained from the optimization problem for 2Tx4Rx

As we can observe in Table 3.3, the value of mutual coherence can be reduced if we decrease the FOV of operation. The lower value of mutual coherence helps us in the stronger signal recovery even in a noisy environment where the MRA-MIMO might fail to recover the original signal. But for short-range applications (large FOV), we do not see significant improvement in the mutual coherence values.

The following figures (ref. Figures :3.4,3.5,3.6) show the relative positions of the synthesized arrays w.r.t the MRA-MIMO for varying Field-of-View.

| 2Tx4Rx | | | | |
|---|----------------|----------------|----------------|---------------|
| Virtual Array Position ($\lambda/2$ units) | | | | |
| Element | FOV | | | MRA |
| | [-15 -15] | [-30 30] | [-50 50] | |
| 1 | 0 | 0 | 0 | 0 |
| 2 | 2.47942 | 1.80411 | 1.01653 | 1 |
| 3 | 5.38293 | 3.28554 | 4.09655 | 4 |
| 4 | 8.69777 | 7.86423 | 6.15630 | 6 |
| 5 | 10.30222 | 11.13576 | 12.84369 | 13 |
| 6 | 12.78164 | 12.93988 | 13.86023 | 14 |
| 7 | 15.68515 | 14.42131 | 16.94025 | 17 |
| 8 | 19 | 19 | 19 | 19 |
| μ | 0.17615 | 0.38734 | 0.48305 | 0.5092 |
| $\mu(dB)$ | -15.08192 | -8.23801 | -6.32002 | -5.8622 |
| Gain (dB) | 9.2197 | 2.3758 | 0.4578 | 0 |

Table 3.3: The Result of the optimization algorithm for 2Tx4Rx

Figure 3.4: Relative position of the synthesized arrays vs MRA for 2Tx4Rx with aperture = $19\lambda/2$

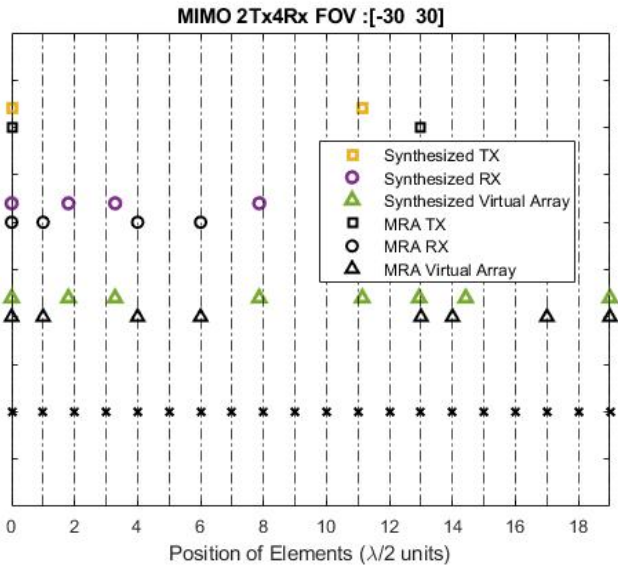


Figure 3.5: Relative position of the synthesized arrays vs MRA for 2Tx4Rx with aperture = $19\lambda/2$

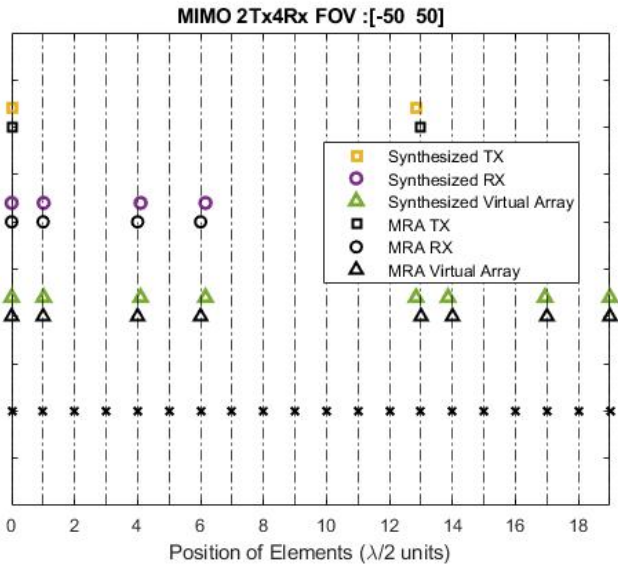


Figure 3.6: Relative position of the synthesized arrays vs MRA for 2Tx4Rx with aperture = $19\lambda/2$

3Tx4Rx - MIMO

Similarly, the synthesis results for 3Tx4Rx MIMO using the optimization problems are summarized in the following tables.

| Position of TX and RX arrays ($\lambda/2$ units) | | | | | | | |
|---|----|--------|---------|----|--------|---------|--------|
| FOV | TX | | | RX | | | |
| | 1 | 2 | 3 | 1 | 2 | 3 | 4 |
| [-15 to 15] | 0 | 7.7040 | 15.3520 | 0 | 2.1676 | 4.3846 | 6.6479 |
| [-30 to 30] | 0 | 8.9322 | 16.5580 | 0 | 1.8714 | 3.8238 | 5.4419 |
| [-50 to 50] | 0 | 7.1718 | 16.8757 | 0 | 3.1101 | 3.99611 | 5.1242 |
| MRA | 0 | 10 | 17 | 0 | 3 | 4 | 5 |

Table 3.4: TX and RX positions obtained from the optimization problem for 3Tx4Rx

| 3Tx4Rx | | | | |
|------------------------|---------------|---------------|---------------|---------------|
| Virtual Array Position | | | | |
| | FOV | | | MRA |
| Element | [-15 to 15] | [-30 to 30] | [-50 to 50] | |
| 1 | 0 | 0 | 0 | 0 |
| 2 | 2.1676 | 1.8714 | 3.1101 | 3 |
| 3 | 4.3846 | 3.8238 | 3.9961 | 4 |
| 4 | 6.6479 | 5.4419 | 5.1242 | 5 |
| 5 | 7.7040 | 8.9322 | 7.1718 | 10 |
| 6 | 9.8716 | 10.8036 | 10.2820 | 13 |
| 7 | 12.0886 | 12.7560 | 11.168 | 14 |
| 8 | 14.3520 | 14.3741 | 12.2961 | 15 |
| 9 | 15.3520 | 16.5580 | 16.8757 | 17 |
| 10 | 17.5196 | 18.4294 | 19.9859 | 20 |
| 11 | 19.7366 | 20.3818 | 20.8718 | 21 |
| 12 | 22 | 22 | 22 | 22 |
| μ | 0.1910 | 0.2551 | 0.3459 | 0.3732 |
| $\mu(dB)$ | -14.3807 | -11.8655 | -9.222 | -8.5612 |
| Gain(dB) | 5.8195 | 3.3043 | 0.6588 | 0 |

Table 3.5: The Result of the optimization algorithm for 3Tx4Rx

It is important to note that the aperture size for synthesizing 3Tx4Rx is set to $22\lambda/2$ which is twice as large as the traditional uniform MIMO with $\lambda/2$ uniform spacing. Double aperture will provide double the angular resolution without adding any extra antenna to the system. But this comes at the cost of increasing mutual coherence (μ) values. Hence, to retain low mutual coherence, the operational Field-of-View needs to get narrower (as observed in table 3.5).

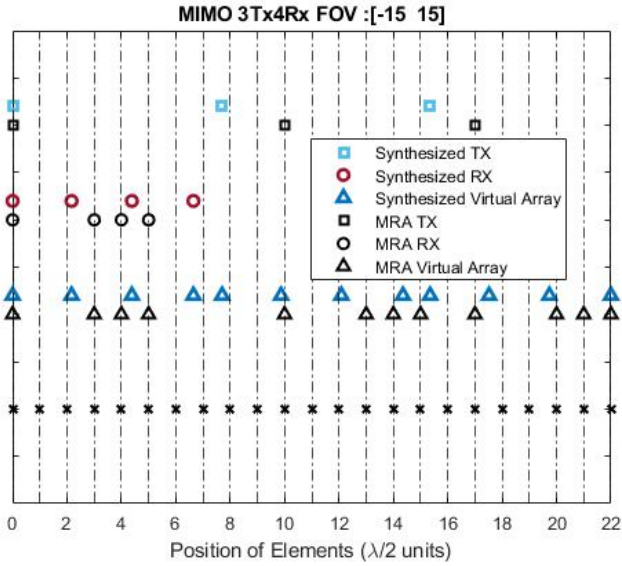


Figure 3.7: Relative position of the synthesized arrays vs MRA for 3Tx4Rx with aperture = $22\lambda/2$

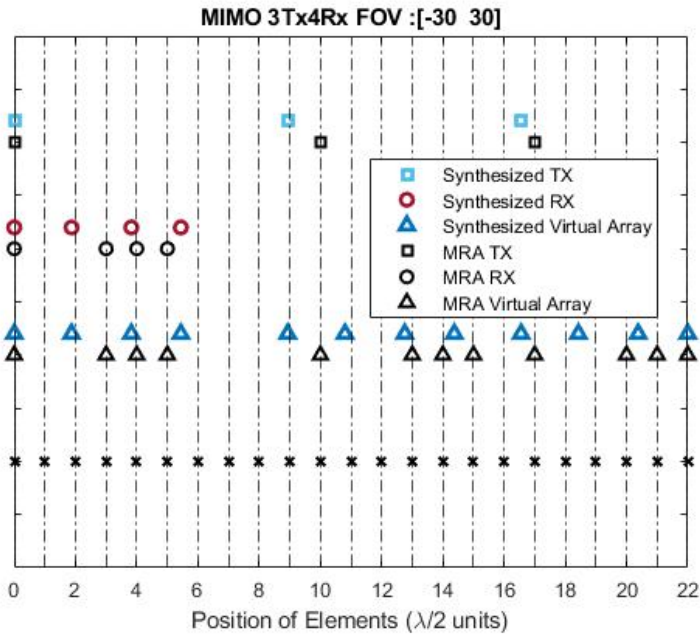


Figure 3.8: Relative position of the synthesized arrays vs MRA for 3Tx4Rx with aperture = $22\lambda/2$

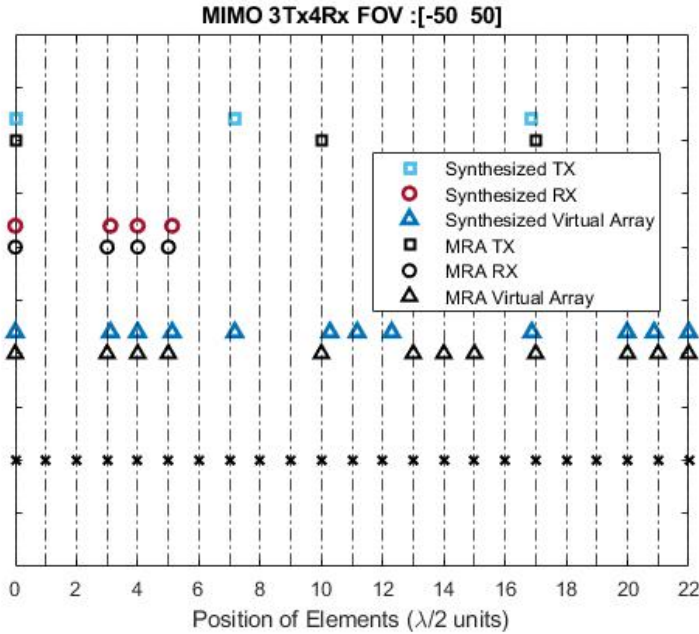


Figure 3.9: Relative position of the synthesized arrays vs MRA for 3Tx4Rx with aperture = $22\lambda/2$

3.5. EXTENSIONS

The iterative optimal topology search algorithm in 3.22 takes the aperture limit (L), the number of transmitters (n_{Tx}) and receivers (n_{Rx}) as the input variables. By interchanging the variables involved, we can extend this iterative optimization technique to obtain additional results useful for antenna design. These extensions will help us analyze the parameters required to meet certain requirement while designing an antenna.

In this section we will look at three possible extensions:

3.5.1. EXTENSION 1

We have formulated the array search algorithm for the MIMO configuration to obtain optimal transmitter and receiver array in 3.22. A similar technique can be applied to obtain an optimal Non-Uniform Linear Array (NULA) of 'M' elements for the desired aperture. In this extension, we will identify the lowest mutual coherence possible for the given number of element 'M,' given aperture size 'L' for a given Field-of-View operation.

The modified optimization problem will be:

$$\begin{aligned}
 & \min_{\epsilon^i} \mu \\
 & s.t. \max |f_{\epsilon_n}^i(\theta_s)| \leq \mu \\
 & |\epsilon^i| \leq \beta, \\
 & D * (\mathbf{x}^{i-1} + \epsilon^i) \geq d_{min} \\
 & |(x_M^{i-1} + \epsilon_M^i) - (x_1^{i-1} + \epsilon_1^i)| = L
 \end{aligned} \tag{3.23}$$

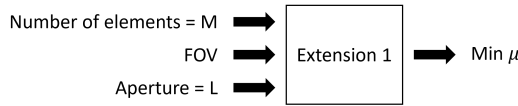


Figure 3.10: The input and the output of the first extension

This optimization is run for varying number of antenna elements for Field-of-View of [-30 to 30] with fixed aperture size of $22\lambda/2$. The result is shown in the Figure 3.11

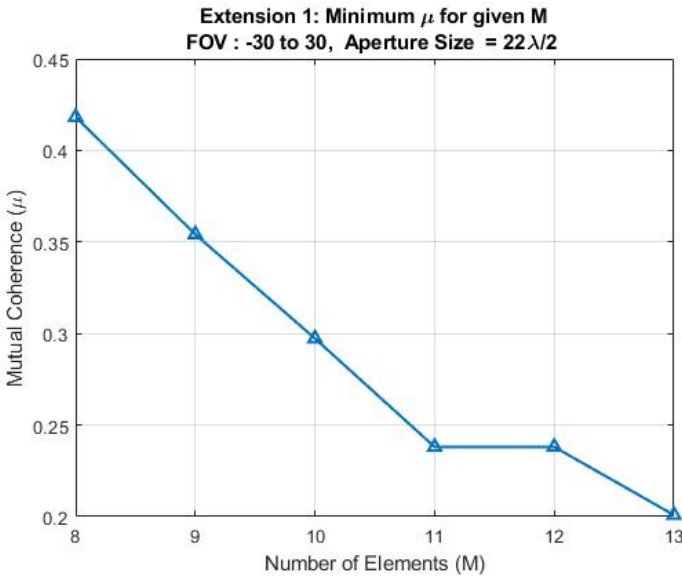


Figure 3.11: Extension 1 Result

As expected, with the increase in the number of elements, the mutual coherence is reduced for the fixed aperture and FOV. This extension can help us determine the lowest possible mutual coherence value for a given number of elements, fixed aperture and FOV.

3.5.2. EXTENSION 2

This extension looks for the largest aperture possible with desired mutual coherence μ value for a fixed number of elements 'M'. Hence, the input to the optimization algorithm will be desired mutual coherence: ' μ ' and the number of elements 'M' for a given Field-of-View. The algorithm's output will be the largest possible aperture size L for the desired constraints.

$$\begin{aligned}
 & \max_{\mathbf{e}^i} L \\
 & s.t. \max |f_{e_n}^i(\theta_s)| \leq \mu \\
 & |\mathbf{e}^i| \leq \beta, \\
 & D * (\mathbf{x}^{i-1} + \mathbf{e}^i) \geq d_{min} \\
 & |(x_M^{i-1} + e_M^i) - (x_1^{i-1} + e_1^i)| \geq L
 \end{aligned} \tag{3.24}$$

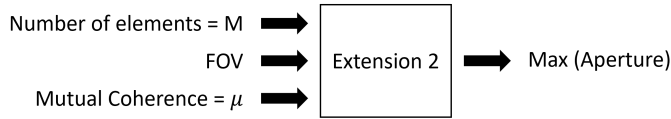


Figure 3.12: The input and the output of the second extension

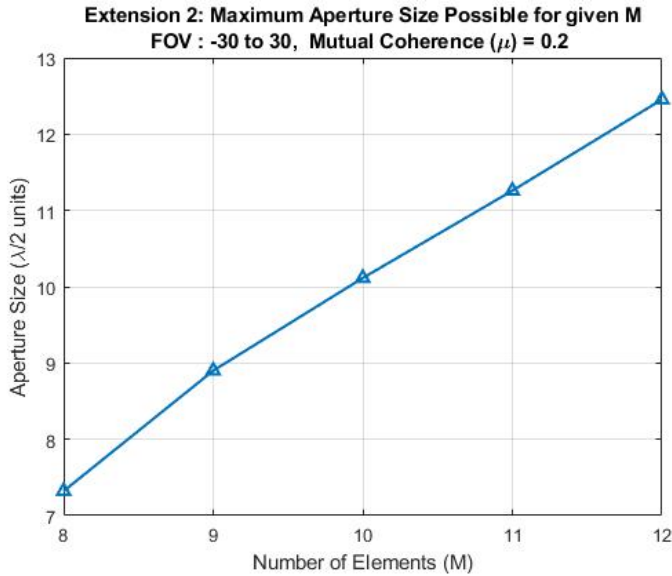


Figure 3.13: Extension 2 Result

As we can see in the figure 3.13, increasing the number of elements can help us achieve larger apertures for the fixed value of mutual coherence.

3.5.3. EXTENSION 3

In this extension, the goal will be to find the minimum number of elements required to achieve certain mutual coherence (μ) and desired aperture size for a given Field-of-View.

$$\begin{aligned}
 &\min \|M\|_1 \\
 &s.t. \max |f_{e_n}^i(\theta_s)| \leq \mu \\
 &\quad |e^i| \leq \beta, \\
 &\quad D * (\mathbf{x}^{i-1} + e^i) \geq d_{min} \\
 &\quad |(x_M^{i-1} + e_M^i) - (x_1^{i-1} + e_1^i)| = L_{min}
 \end{aligned} \tag{3.25}$$

The actual goal function should be l_0 -norm of M i.e. $\|M\|_0$ but this makes the problem non-convex. Hence, we will use $\|M\|_1$, the l_1 -norm of M as our goal function.

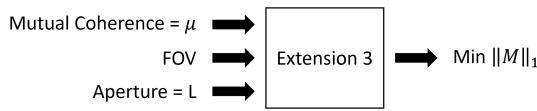


Figure 3.14: The input and the output of the second extension

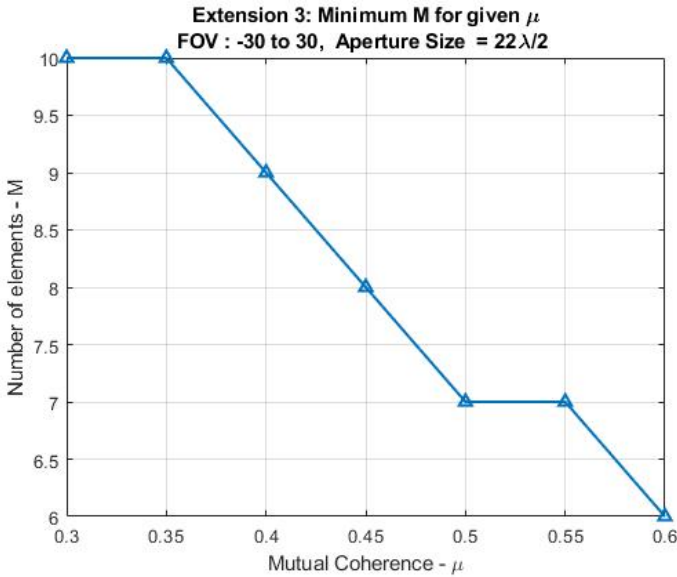


Figure 3.15: Extension 3 Result

3.6. CONCLUSION

This chapter proposed two techniques to design Sparse-MIMO to minimize the Mutual Coherence (μ) value. Minimizing the μ provides a stronger recovery guarantee of the signal using sparse recovery algorithms. Also, making the array sparse improves the array's aperture, and thus the angular resolution is also improved.

The first technique is a Grid-based topology search for the lowest mutual coherence. This technique scans through possible transmitter and receiver antennas at specific grid points with uniform spacings, meeting aperture size requirements. Then, the transmitter (TX) and receiver (RX) arrays for MIMO with the lowest mutual coherence are selected.

The second technique is a Grid-less Optimal topology search, based on an iterative convex optimization algorithm. The positions of the antenna elements are updated at each iteration in the direction of the topology that gives a lower mutual coherence value. The iterative optimization algorithm is computationally effective and can provide near-optimal solutions. This method may get stuck at local optima, and in order to avoid that Simulated Annealing technique is used to achieve global optima.

The design techniques introduced in this chapter focus on optimizing the physical locations of the transmitter and receiver array rather than the virtual array since it is possible that the optimum virtual array does not have the realizable receiver and transmitter arrays.

The iterative optimization algorithm can be applied to our problem and get additional results. The extensions introduced in this chapter will help analyze the relationship between various parameters, and depending on the requirements and constraints, one can select a specific extension to check the limits.

4

SUPER RESOLUTION DOA ESTIMATION

This chapter will focus on the Direction-of-Arrival (DOA) estimation of the targets. It is important to note that we will be using just a single snapshot of received data to make quick decisions in time-critical applications. At the same time, the goal is to achieve super-resolution estimates with high confidence.

A class of DOA estimation algorithms has shown promising results using a single snapshot without compromising the angular resolution. This class is known as Sparse Recovery Algorithms. In the previous chapter, we discussed the techniques to design MIMO arrays with low mutual coherence. We have seen that a lower mutual coherence value provide a higher guarantee for recovery of sparse signals. Hence, we expect the designed MIMO arrays from the previous chapter to give the best performance for sparse recovery algorithms.

First, we will formulate the DOA estimation problem into a sparse recovery problem and summarize the prominent Sparse Recovery Algorithms available in the literature. We will use the possible candidates suitable for automotive application and compare their performances against each other in order to determine the optimal algorithm.

4.1. DOA ESTIMATION USING SPARSE RECOVERY

In this section we will introduce the sparse representation of our signal model. As we have defined earlier, for K targets, the signal model with single snapshot contains corresponding K steering vectors, forming the steering matrix $\mathbf{A}_s \in \mathbb{C}^{M \times K}$ (Figure 4.1). The vector $\mathbf{s}_s \in \mathbb{C}^K$ contains the reflected complex signal from each target and $\mathbf{W} \in \mathbb{C}^M$ contains the noise information.

$$\mathbf{y} = \mathbf{A}_s \mathbf{s}_s + \mathbf{W} \tag{4.1}$$

This signal model can be represented in sparse domain, if we consider that the \mathbf{A}_s can be formed by selecting specific columns from a larger dictionary $\mathbf{A} \in \mathbb{C}^{M \times N}$ whose

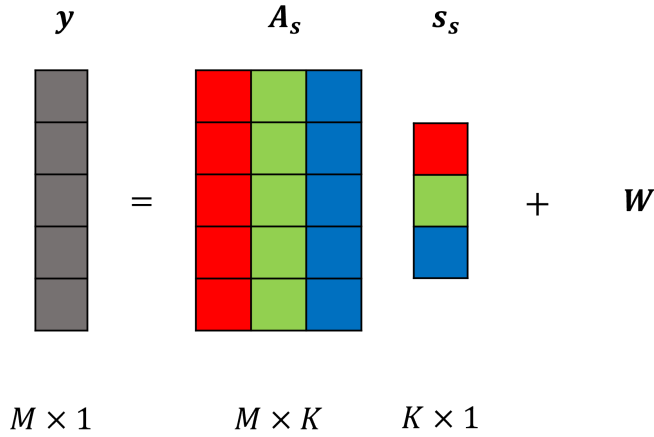


Figure 4.1: Signal Model for K-targets

columns are called atoms. Similarly the corresponding $\mathbf{s} \in \mathbb{C}^N$ will become the selection vector that selects respective atoms from \mathbf{A} and linearly combine them to form $\mathbf{y} \in \mathbb{C}^M$ (Figure 4.2). By sparsity, we mean that only a few entries, say $K \ll N$, of \mathbf{s} are non-zero and the rest are zero. This is true for our signal model since the number of targets (K) is \ll the total possible positions (N) in angular domain.

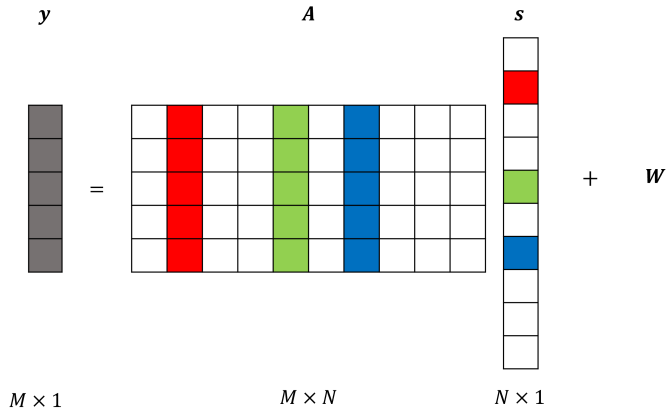


Figure 4.2: Sparse Representation of the signal model containing K-targets

Given \mathbf{y} and \mathbf{A} , the problem of sparse recovery is to find the sparse vector \mathbf{s} subject to data consistency. But since, for DOA estimation we are only concerned with the non-zero locations of the sparse vector \mathbf{s} , the sparse recovery algorithms will focus on finding the support of $\mathbf{s} = \text{supp}(\mathbf{s}) = \text{locations/indices of the non-zero locations of the vector } \mathbf{s}$.

Intuitively, the sparsest solution to solve for the sparse signal should be found. So, if

the noise is absent, the following optimization problem should be solved:

$$\mathbf{s} = \underset{\mathbf{s}}{\operatorname{argmin}} \|\mathbf{s}\|_0 \quad \text{subject to } \mathbf{y} = \mathbf{A}\mathbf{s}; \quad (4.2)$$

The l_0 problem in 4.2 is NP-hard to solve. So, a more efficient approach is needed to solve this problem. In the literature, there have been many methods and algorithms proposed to solve for sparse signal recovery. The next section will briefly look at the different approaches and select possible candidates suitable for automotive application.

4.2. SPARSE RECOVERY ALGORITHMS

In this section, we will summarize the popular algorithms for sparse recovery. The goal of sparse recovery algorithms is to find the sparsest solution to the problem 4.2. The steering matrix \mathbf{A} can be created with discrete or continuous atoms. Hence, the sparse recovery algorithms on the broader scope can be divided into three major categories:

4.2.1. GRID-BASED ALGORITHMS

In this category, the algorithms will use the dictionary \mathbf{A} based on the discrete atoms and hence the term 'Grid-based' algorithms. There has been extensive research done on sparse recovery algorithms. These algorithms can be classified under six approaches. A summary of these approaches with their Pros and Cons are listed in Table 4.1. Readers can consult [5], [35] for a review.

Automotive applications desire to estimate the Direction-of-Arrival (DOA) targets in a noisy environment using a single snapshot. As we can see from Table 4.1, the Combinatorial approach requires noiseless measurements and works best when there is a specific pattern in measurements [36]. Similarly, the Bayesian approach demands prior information on the signals and expects the signal belonging to some known probability distribution [37]. Since we are working with single snapshots, the Bayesian approach will not be efficient. Hence we can discard these two approaches from our analysis.

For the rest, we will select the most popular algorithm with low complexity and high-resolution algorithms from each approach and compare their performance.

CONVEX APPROACH

This approach poses sparse recovery problem as a convex optimization algorithms which can be solved using off-the-shelf solvers [33]. One of the most popular algorithm from this category is:

Basis Pursuit Denoising (BPDN): BPDN was introduced by Chen *et. al* [38]. This is similar to the Least Absolute Shrinkage Selection Operator (LASSO) algorithm, introduced by Tibshirani [39] in statistics. BPDN considers the noise in measurements and formulates the optimization problem given by 4.3.

$$\hat{\mathbf{s}} = \underset{\mathbf{s}}{\operatorname{argmin}} \|\mathbf{s}\|_0; \quad \text{subject to } \frac{1}{2} \|\mathbf{y} - \mathbf{A}\mathbf{s}\|_2^2 \leq \epsilon, \quad (4.3)$$

Some algorithms solve BPDN using Lagrangian form, which can be formulated as 4.4, where λ is unknown prior. The value of λ is used to balance the sparsity of the solution

| Approach | Complexity | Attributes | Pros | Cons |
|---------------|--|--|--|---|
| Convex | $\approx O(m^2 n^3)$ | - global optimization - minimizes l_1 -norm | - robust to noise - ability to superresolve | - slower, complex |
| Greedy | -serial version: $O(mnk)$ -parallel version: $O(mn.iter)$ | - correlation based step-by-step iterative method | - faster, low complex, robust to noise - parallel versions can discard wrong entries from previous iterations | - prior knowledge on sparsity required - convergence issues, requires more measurements than convex approach |
| Thresholding | $O(mn.iter)$ | - nonlinear thresholding criteria to select atoms | -faster, low complex | - convergence issue - requires adaptive step size |
| Combinatorial | linear in n | - min and median computation | - faster, simple | - requires noiseless measurements - specific pattern in measurements required |
| Non-Convex | $\approx O(m^2 n^3)$ | - minimizes l_p -norm where $0 < p < 1$ | - recovers from fewer measurements - functions under weaker RIP | - slower, complex |
| Bayesian | $O(nm^2)$ | - recovery for bayesian inference problem - applicable for signals \in known probability distribution | - faster & more sparse solution | - prior dependent -high computation |

Table 4.1: Summary of Sparse Recovery Approaches

and error. To solve 4.4, one of the famous algorithms is the primal-dual interior-point method.

$$\hat{\mathbf{s}} = \arg \min_{\mathbf{s}} \lambda \|\mathbf{s}\|_0; \quad \text{subject to} \quad \frac{1}{2} \|\mathbf{y} - \mathbf{A}\mathbf{s}\|_2^2 \leq \epsilon, \quad (4.4)$$

4.2.2. GREEDY APPROACH

Whereas, Greedy Approach is a step-by-step iterative method.

The convex optimization approach is a global optimization method. At each iteration, the solution is formed by selecting the columns from the dictionary matrix (steering matrix), which are highly correlated with the measurement. These selected columns are called atoms. The atoms selected at each iteration are removed to improve the reconstruction, reducing the algorithm's computational complexity. Hence these algorithms are considered as a fast and straightforward approach for sparse reconstruction.

These algorithms are further divided into two categories:

1. Serial Greedy Algorithm: The Orthogonal Matching Pursuit (OMP) proposed by Y. C. Pati *et al.* [40] can be considered as a Serial Greedy Algorithm. Only one atom is selected in each algorithm iteration, and the respective support vector (indices of non-zero entries of solution) is calculated. The steps:

- *Initialization:* A residual vector r is initialized with measurement vector \mathbf{y} . Solution vector \mathbf{s} and support vector Λ are initialized to null vectors. And the iteration is started.
- *Atom Search:* This step search for the column of dictionary matrix which is maximally correlated to the residual vector. The position/index of this atom is stored in Λ .
- *Update the solution:* The solution set is updated is using Least Squares Method, \mathbf{s}_i
- *Update the residual:* New residual is calculated by subtracting $\mathbf{A}_{\Lambda_i} \mathbf{s}_i$ from the measurement vector \mathbf{y} . For convergence, these steps are either repeated for K times or desired value of residual is reached.

2. Parallel Greedy Algorithm: The Compressive Sampling Matching Pursuit (OcSaMP) proposed by Needell and Tropp [41] can be categorized as Parallel Greedy Algorithm. Unlike OMP, each iteration of CoSaMP selects $2K$ columns from the A , which are maximally correlated with the residual vector. These are added to the K atoms from the previous iteration. Best K atoms are retained from these $3K$ atoms, by least-squares best fit for sparse vector \mathbf{s} . Then the locations of these atoms are updated in Λ .

THRESHOLDING APPROACH

In this approach, the algorithms work with K atoms simultaneously. A thresholding operation is performed to update the solution set \mathbf{s}_i . The rest of the steps are similar to the Greedy Approach. One of the most popular thresholding algorithms is:

Iterative Hard Thresholding Algorithm (IHT): Blumensath and Davies proposed the IHT algorithm [42]. This method selects a thresholding operator p_k to keep largest K entries in \mathbf{s} and the rest is set to zero.

$$\mathbf{s} = p_k(\mathbf{s} + \lambda \mathbf{A}^T(\mathbf{y} - \mathbf{A}\mathbf{s})) \quad (4.5)$$

The λ denotes the step size of the iterations. There are algorithms with adaptive step sizes to converge faster, but it becomes more complicated.

NON-CONVEX APPROACH

The sparse recovery algorithms try to find the sparsest solution, basically minimizing the l_0 -norm. But it is an NP-hard problem. The convex approach relaxes the l_0 -norm to $l_{1/2}$ -norm optimization problem. Whereas, in the non-convex approach l_1 -norm is replaced with l_p -norm where, $0 < p < 1$. The advantage of this approach is that we can reconstruct the sparse signal with fewer measurements than the convex counterpart. This approach also works with a weaker RIP conditioned dictionary matrix. The most popular algorithm in this category is:

Focal Underdetermined System Solution (FOCUSS): Gorodnitsky and Rao proposed the FOCUSS algorithm [43]. This method is the non-convex relaxation of the l_0 -norm optimization problem. The optimization problem is given by 4.6

$$\hat{\mathbf{s}} = \underset{\mathbf{s}}{\operatorname{argmin}} \|\mathbf{s}\|_p \quad \text{subject to } \mathbf{y} = \mathbf{A}\mathbf{s}; \quad (4.6)$$

In order to guarantee convergence, a regularized FOCUSS was introduced in [44]. The regularized version is given by

$$\hat{\mathbf{s}} = \underset{\mathbf{s}}{\operatorname{argmin}} \lambda \|\mathbf{s}\|_p + \frac{1}{2} \|\mathbf{A}\mathbf{s} - \mathbf{y}\|^2 \quad (4.7)$$

where $\lambda > 0$ is a regularization parameter.

4

4.2.3. OFF-GRID ALGORITHMS

These algorithms focus on a dynamic grid for the atoms. But most of these algorithms involve non-convex optimization, and only local convergence can be guaranteed. Hence this category will not be the focus of our analysis.

4.2.4. GRIDLESS ALGORITHMS

In this section, the DOA estimation approach designated as the sparse gridless method is presented. As the name suggests, this method does not require gridding of the direction domain. Instead, it directly operates in the continuous domain and can resolve the grid mismatch problem while sparse recovery. Moreover, it is convex and has strong theoretical guarantees. However, this kind of method can only be applied to uniform or sparse linear arrays on a uniform grid.

ATOMIC NORM

Atomic norm is analogous to l_0 -norm minimization from grid-based methods. The problem is formulated as frequency estimation for DOA. The optimization problem can be given by 4.8.

$$\hat{\mathbf{s}} = \underset{\mathbf{s}}{\operatorname{argmin}} \|\mathbf{s}\|_A \quad \text{subject to } \mathbf{y} = \mathbf{A}\mathbf{s}; \quad (4.8)$$

where, $\|\cdot\|_A$ means the atomic-norm.

There have been different approaches proposed in the literature to solve optimization problems 4.8. Reader can review in [45], [46]. However, most of them have focused on ULA and Sparse Linear Arrays on a grid. And the proposed Array Topology optimization results in Non-Uniform Sparse Arrays, for which there is not much literature available to implement atomic norm optimization. There have been few techniques given by [47],[48], but these techniques either increase computational complexity or move away from the grid-less approach.

4.3. TRADITIONAL DOA ESTIMATION ALGORITHMS

Until now, we saw the sparse recovery algorithms for single snapshot DOA estimation. The state-of-art high-resolution subspace-based algorithms such as Multiple Signal Clas-

sification (MUSIC), Root-MUSIC, Minimum Variance Distortionless Response (MVDR/Capon), etc., require multiple snapshots in order to estimate DOAs correctly.

Some advanced algorithms have been proposed to estimate DOA using Single Snapshots in [49–52]. But these algorithms exploit the Uniform Linear Array structures and compromise on the angular resolution as well. For Non-Uniform Linear Arrays, it is not easy to adapt these advanced algorithms.

4.3.1. DETERMINISTIC MAXIMUM LIKELIHOOD ESTIMATOR (DML):

Stoica and Sharman proposed DML for DOA estimation in [53]. DML algorithm is robust to noise and is considered the best estimator for DOA estimation. DML finds the vector \mathbf{s} that maximizes the negative of the log-likelihood function 4.9 [54].

$$L = -\log(\sigma^2) - \frac{1}{\sigma^2} \sum_{i=1}^N |\mathbf{y} - \mathbf{A}\mathbf{s}|^2 \quad (4.9)$$

where N = number of snapshots = 1 for our case.

Since the logarithm is a monotonic function, the maximization problem is simplified to

$$\arg \min_{\theta, \mathbf{s}} |\mathbf{y} - \mathbf{A}(\theta)\mathbf{s}| \quad (4.10)$$

where θ is the set of True DOAs of the targets. After simplifying, the maximum likelihood estimate of the parameter Θ is obtained by maximizing the log-likelihood function:

$$\mathbf{L}(\theta) = |\mathbf{P}_{\mathbf{A}(\theta)}\mathbf{Y}|^2 \quad (4.11)$$

where,

$$\mathbf{P}_{\mathbf{A}(\theta)} = \mathbf{A}(\theta)(\mathbf{A}^H(\theta)\mathbf{A}(\theta))^{-1}\mathbf{A}^H(\theta) \quad (4.12)$$

The simplified version of equation 4.11 is given by

$$\mathbf{L}(\theta) = \text{tr}[\mathbf{P}_{\mathbf{A}(\theta)}\mathbf{R}] \quad (4.13)$$

where $\text{tr}[\]$ is trace of the bracketed matrix and the \mathbf{R} is the sample covariance matrix.

$$\mathbf{R} = \mathbf{y} * \mathbf{y}^H; \quad (4.14)$$

(since we have only one snapshot).

4.4. PERFORMANCE ANALYSIS

In this section, we will test the performance of the algorithms we discussed in the previous sections. These algorithms will be tested on the synthesized arrays compared based on their angular resolution, Probability of Detection and SNR performance. For the following analysis, the synthesized grid-based optimal array will be referred to as Minimum Redundancy MIMO (MRA-MIMO). The synthesized arrays will be compared against Uniform Linear MIMO Array having some number of transmitters and receivers.

4.4.1. PROBABILITY OF DETECTION

Probability of Detection (P_D) is defined as the probability of the algorithm to estimate DOAs of the targets within an acceptable error margin. This simulation will determine the P_D for each algorithm and compare their performance against the synthesized arrays and the existing MIMO array (ULA-MIMO).

For the simulation setup, we will place two targets symmetric to the broadside direction. The targets will move away from each other, and at each angular separation, the algorithms will estimate the target location. The simulation is run for 1000 iterations for varying Signal-to-Noise Ratio, and the error margin is set ≤ 0.25 degrees to obtain Probability of Detection (P_D).

The key plots are shown in the following figures:

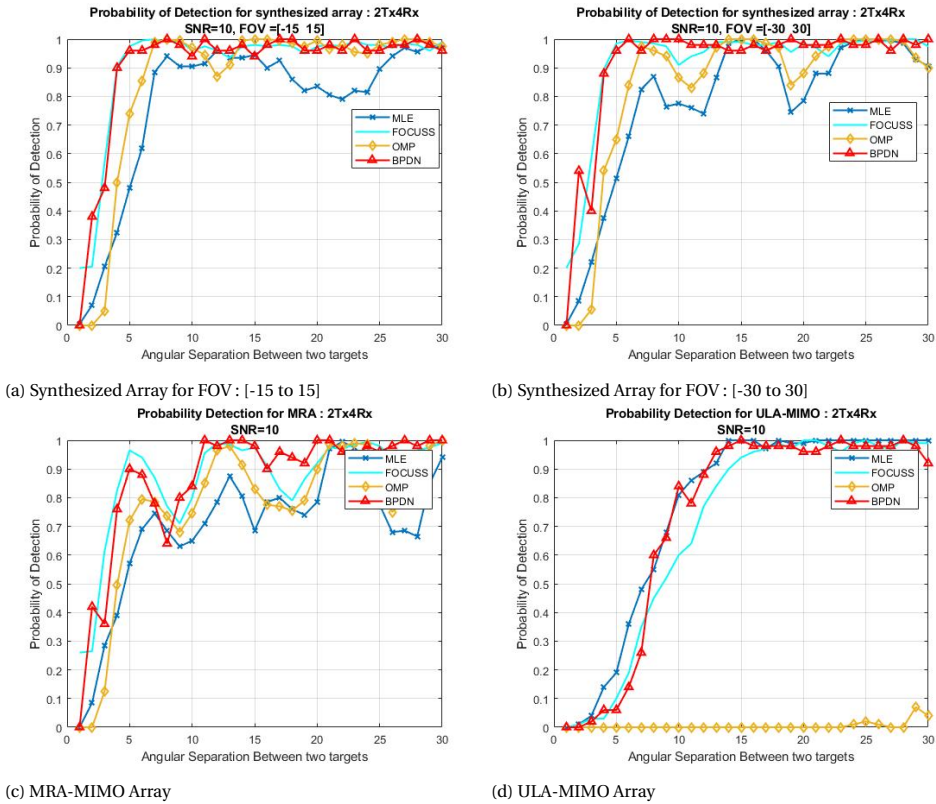


Figure 4.3: Probability of Detection of the arrays for 2Tx4Rx at SNR = 10dB

From the plots, 4.3 and 4.4 following observations can be made:

- MLE, FOCUSS, OMP and BPDN were able to perform the best among the selected candidates for analysis.
- At low SNR values, Synthesized arrays have shown consistent and high probability

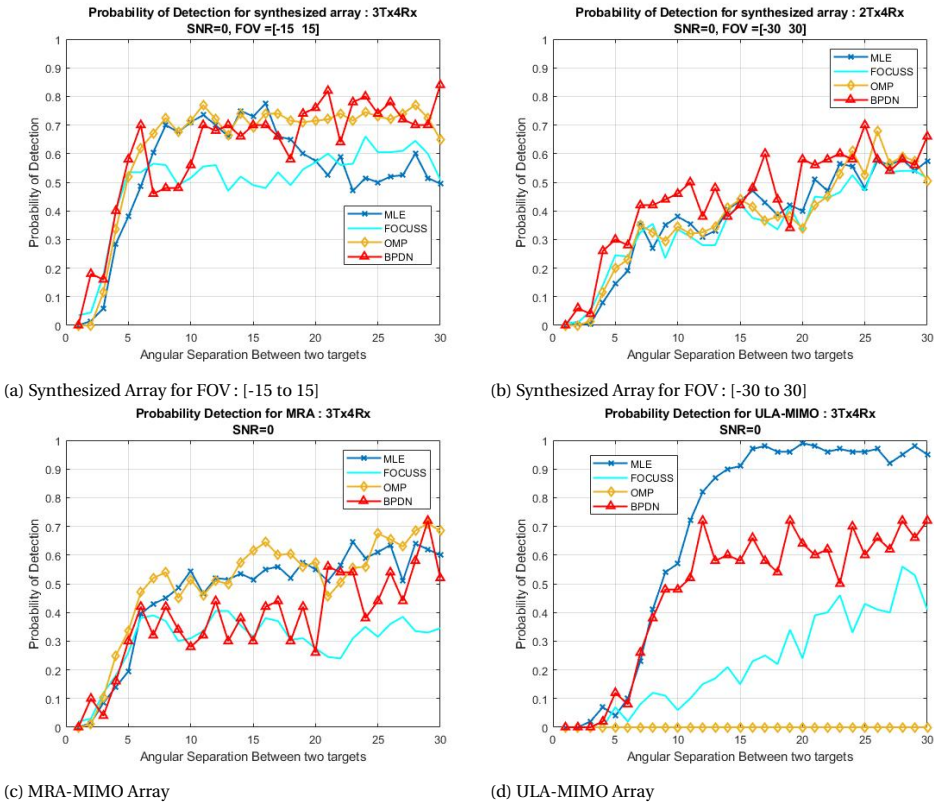


Figure 4.4: Probability of Detection of the arrays for 3Tx4Rx at SNR = 0dB

of detection (P_D) compared to MRA and ULA MIMO (Figure : 4.3a, 4.4a).

- Synthesized arrays have improved angular resolution compared to ULA-MIMO.
- Even though BPDN shows high-resolution performance, it does not seem stable.
- OMP performance is bad with ULA but it performs well with synthesized arrays (Figure 4.3a).
- BPDN struggles to show consistent performance at low SNR values.

4.4.2. ANGULAR RESOLUTION

The Angular Resolution of the algorithm for each respective array is determined with the help of Probability of Detection (P_D). The results from the previous simulations are used to determine the resolution. In order to find the resolution, we set the following condition: if the $P_D \geq 0.98$, then the two targets are successfully resolved in angular domain, and the separation between those targets will be defined as the Angular Resolution of the algorithm for the respective array.

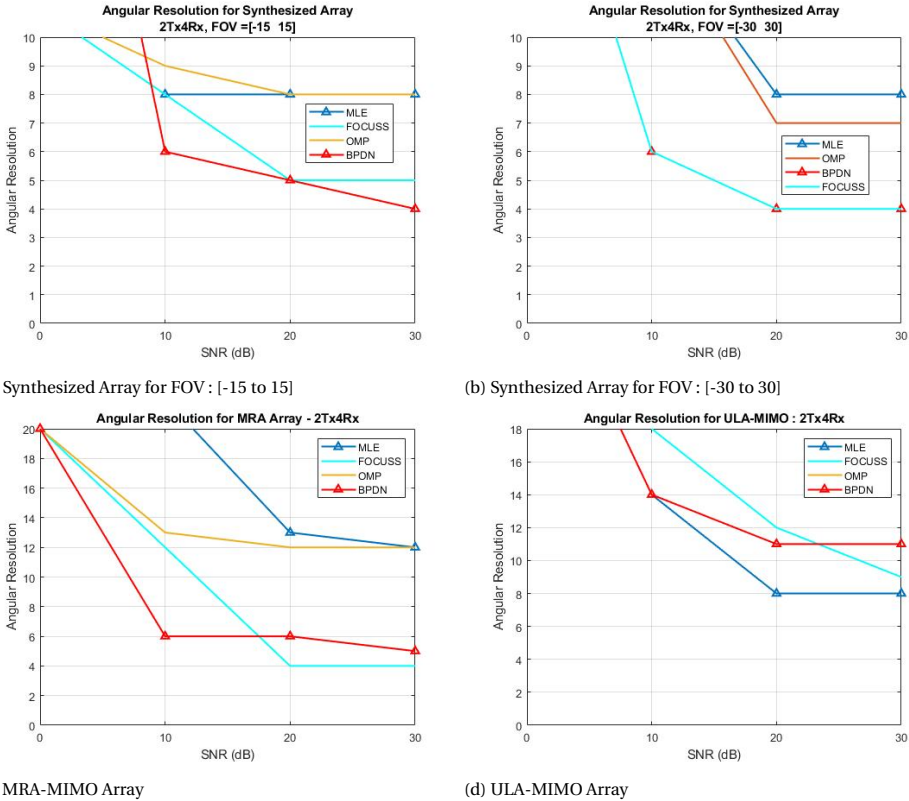
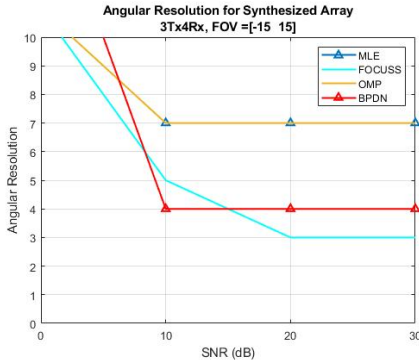
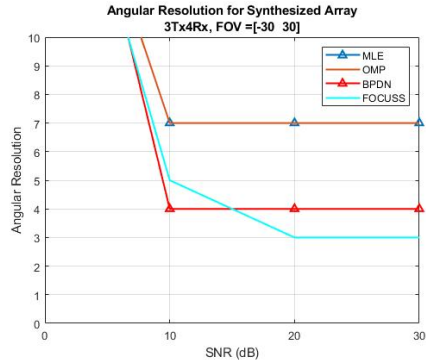


Figure 4.5: Angular Resolution performance of the arrays for 2Tx4Rx

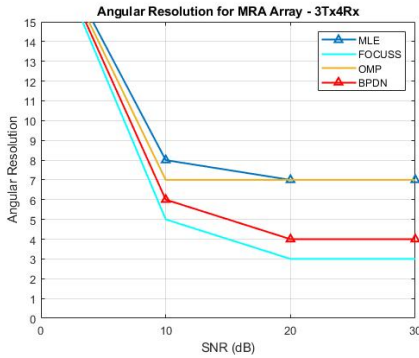
In Figure 4.5, the angular resolution of each algorithm for varying SNR values is calculated. For MRA-MIMO and synthesized arrays, the sparse recovery algorithms BPDN and FOCUSS provide super-resolution. And for ULA-MIMO, MLE performs the best for resolving two targets.



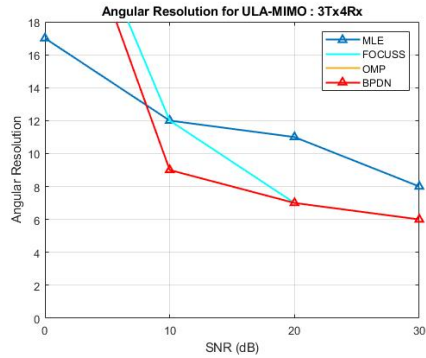
(a) Synthesized Array for FOV : [-15 to 15]



(b) Synthesized Array for FOV : [-30 to 30]



(c) MRA-MIMO Array



(d) ULA-MIMO Array

Figure 4.6: Angular Resolution performance of the arrays for 3Tx4Rx

From Figure 4.6, it is clear that the FOCUSS performs better at high SNR values and BPDN performs better at low SNR range. A complex algorithm like MLE is performing at the same range of simple algorithm like OMP for for the synthesized arrays.

SUMMARY

The results from the previous plots are summarized in the following tables. The synthesized MIMO arrays improve up to 2° in angular resolution with respect to the MRA-MIMO and up to 8° w.r.t. ULA-MIMO. It is important to note that the MRA-MIMO has the same performance as the synthesized arrays, but in the low SNR region, the proposed arrays have better resolution.

| Angular Resolution (2Tx4Rx) | | | | | |
|-----------------------------|--------------------|-----------------|-----------------|-----|----------|
| - | Synthesized Arrays | | | | |
| SNR (dB) | FOV [-15 to 15] | FOV [-30 to 30] | FOV [-50 to 50] | MRA | ULA-MIMO |
| 10 | 6 | 6 | 6 | 7 | 14 |
| 20 | 4 | 4 | 4 | 6 | 8 |
| 30 | 4 | 4 | 4 | 4 | 8 |

Table 4.2: Summary of the Angular Resolution of the Arrays for 2Tx4Rx.

| Angular Resolution (3Tx4Rx) | | | | | |
|-----------------------------|--------------------|-----------------|-----------------|-----|----------|
| - | Synthesized Arrays | | | | |
| SNR (dB) | FOV [-15 to 15] | FOV [-30 to 30] | FOV [-50 to 50] | MRA | ULA-MIMO |
| 10 | 4 | 4 | 6 | 6 | 9 |
| 20 | 3 | 3 | 3 | 4 | 7 |
| 30 | 3 | 3 | 3 | 3 | 6 |

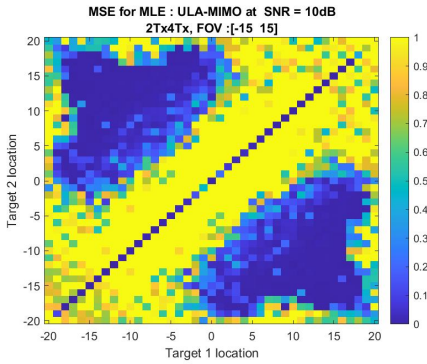
Table 4.3: Summary of the Angular Resolution of the Arrays for 3Tx4Rx.

4.4.3. COMBINED PERFORMANCE

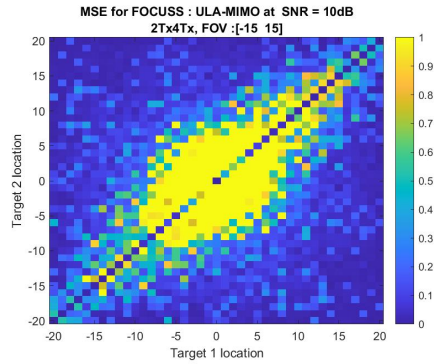
In this simulation, the performance of two algorithms will be tested. The goal of the simulation is to show the super-resolution performance of the sparse recovery algorithm FOCUSS coupled with the synthesized MIMO arrays. It will be compared against the standard MLE algorithm.

For this simulation, two targets are scanned throughout specified FOV (e.g. [-20 to 20]). The two targets take all possible positions within the FOV, and the algorithms perform the DOA estimation for two targets. The MSE over 100 iterations have been averaged and plotted in the following figures. On the left side, the performance of the MLE algorithm is plotted, and FOCUSS is plotted on the right side. These algorithms are tested for synthesized arrays, MRA-MIMO and ULA-MIMO for both 2Tx4Rx and 3Tx4Rx configurations.

The advantage of sparse recovery algorithm FOCUSS can be seen on the right side figures. Even for ULA-MIMO, the FOCUSS shows good performance (Figure 4.7a). The MSE for synthesized arrays is much lower than the counterparts for both of the algorithms. The combined result of the sparse-recovery algorithm and the synthesized array can be observed in Figure 4.9b.

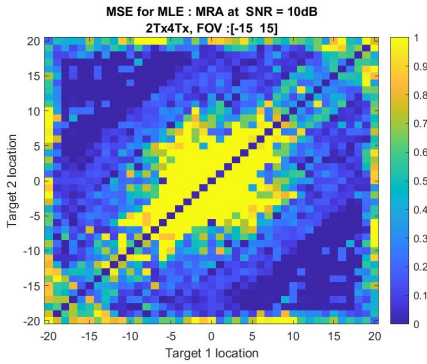


(a) Performance for MLE

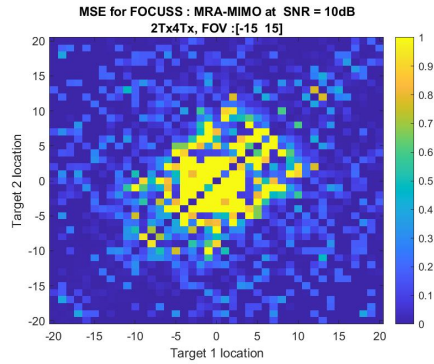


(b) Performance for FOCUSS

Figure 4.7: MSE for ULA : 2Tx4Rx

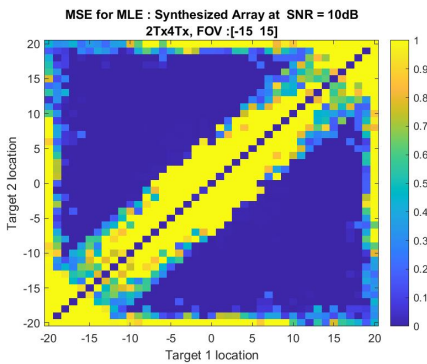


(a) Performance for MLE

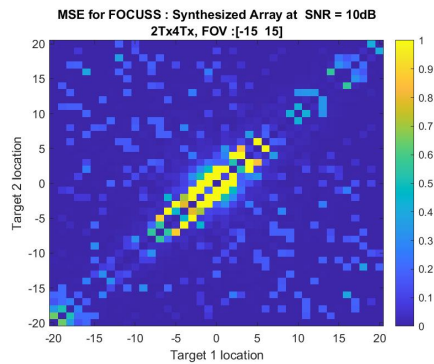


(b) Performance for FOCUSS

Figure 4.8: MSE for MRA-MIMO : 2Tx4Rx

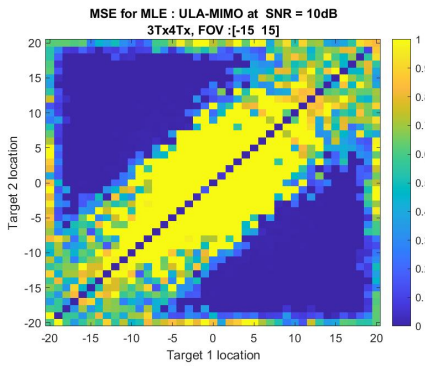


(a) Performance for MLE

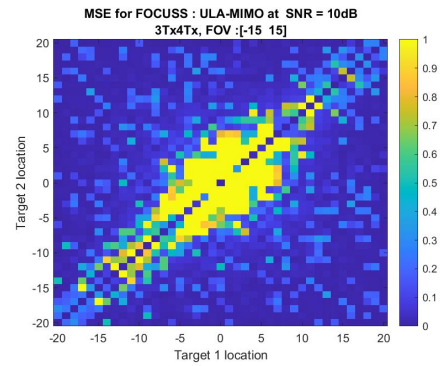


(b) Performance for FOCUSS

Figure 4.9: MSE for Synthesized MIMO : 2Tx4Rx

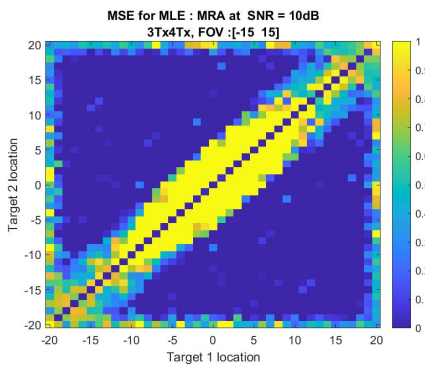


(a) Performance for MLE

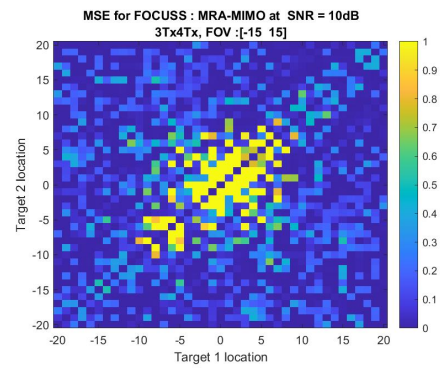


(b) Performance for FOCUSS

Figure 4.10: MSE for ULA -MIMO : 3Tx4Rx

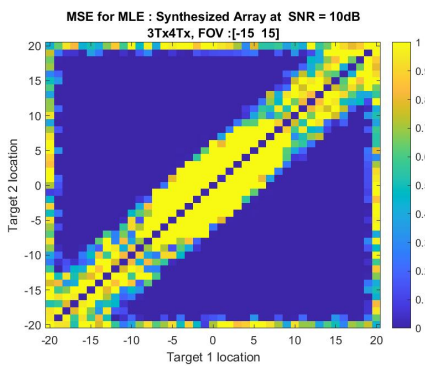


(a) Performance for MLE

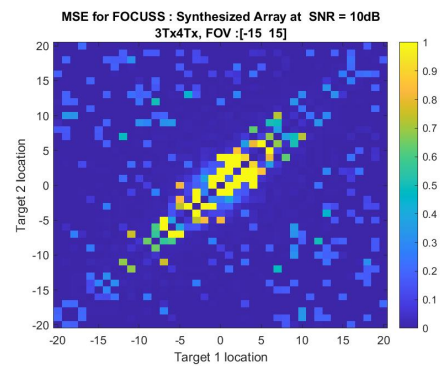


(b) Performance for FOCUSS

Figure 4.11: MSE for MRA-MIMO : 3Tx4Rx



(a) Performance for MLE



(b) Performance for FOCUSS

Figure 4.12: MSE for Synthesized MIMO : 3Tx4Rx

4.5. CONCLUSION

In this chapter, different approaches for sparse recovery are studied, and prominent sparse recovery algorithms are selected for testing against the synthesized arrays. The Probability of Detection (P_D) is an important feature to describe the algorithm's reliability. The BPDN, FOCUSS, MLE and OMP have shown high P_D values in a single snapshot case. The synthesized arrays provided higher P_D in the low SNR region compared to MRA-MIMO and ULA-MIMO. P_D can be used to determine the angular resolution of the algorithms. Two targets are considered resolved if the $P_D \geq 0.98$ at that angular location. With such a high confidence rate, BPDN and FOCUSS provided the highest resolution of 4° for synthesized 2Tx4Rx array and 3° for synthesized 3Tx4Rx array, which is twice the improvement over the ULA-MIMO array. Both of these algorithms have the same complexity, and the choice of selection depends on the noise level of the environment and expected resolution.

The combined effect of synthesized MIMO and sparse recovery algorithm is analyzed. The synthesized arrays start to show better performance in the low-SNR region ($10dB$). For both synthesized arrays, 2° of improved angular resolution over MRA-MIMO at low-SNR is observed. The synthesized arrays have consistent performance with high accuracy of the estimations within the field of view.

5

CONCLUSION AND FUTURE WORK

5.1. CONCLUSIONS

This thesis considered different design techniques for Sparse-MIMO Array, and the sparse recovery algorithms' performance was analyzed. The goal of the thesis is to design a Sparse-MIMO Array with low Mutual Coherence values such that the recovery performance of the sparse recovery algorithm is improved. Two distinct techniques for designing transmitter (Tx) and receiver (Rx) arrays to obtain MIMO with low mutual coherence value are analyzed. The first technique, grid-based search for optimal array topology, restricts the antenna elements' location on a fixed grid. And the second technique is a grid-less search for the optimal location of the elements.

For the grid-based search, it was possible to run an exhaustive search and look for the topology with the lowest mutual coherence value. This search leads towards the Restricted-Minimum Redundancy MIMO (MRA-MIMO). However, for grid-less optimal array search, the exhaustive search is not possible. From different techniques available to search grid-less array topology, the convex optimization technique was selected. This technique is computationally efficient and has been proven to provide near-optimal solutions. Hence, based on the convex optimization technique, an algorithm to search MIMO configuration with mutual coherence as the cost function is proposed.

The existing optimization approaches for MIMO optimize the virtual array element positions and then recover Tx and Rx arrays. The proposed novel optimization algorithm looks for sparse arrays with user-specified aperture size and optimizes Tx and Rx array elements' positions rather than virtual array element position. Therefore, the approach proposed provides Tx and Rx array elements' positions as output without the need for further processing. Thus, the optimization algorithm requires the input of the number of transmitters, number of receivers, Field-of-View of operation and the aperture size and returns the optimal transmitter and receiver array topologies.

The algorithm might get stuck at local optima since the optimization problem is solved using the interior-point method. In order to avoid that, the simulated annealing method was implemented to add an extra layer of robustness to the proposed algorithm.

The most common MIMO configurations in automotive radar are 2Tx4Rx and 3Tx4Rx with short-range, medium-range, and long-range operations. The optimization algorithm was run for these configurations with different field-of-view depending on the range of operation. The synthesized arrays with the smallest FOV (long-range application) dramatically improved mutual coherence values compared to the existing grid-based optimal MIMO (MRA-MIMO). We observed the gain up to 9.2dB for 2Tx4Rx and up to 5.82dB for 3Tx4Rx. The proposed algorithm also provided some extensions that might be helpful for antenna designers. These extensions gave us the limits of operation for aperture, the number of elements and mutual coherence.

After successfully synthesizing MIMO arrays with low mutual coherence values, it is necessary to couple them with super-resolution algorithms for DOA estimation to achieve the best performance. Prominent sparse recovery algorithms are selected for testing the performance of the synthesized arrays. These algorithms are tested based on Probability of Detection (P_D), Angular Resolution and Estimation Accuracy to find the optimal algorithm for the synthesized arrays.

At high SNR range (30dB), synthesized MIMO arrays provided 4° (twice) improvement in angular resolution over ULA-MIMO. Whereas MRA-MIMO and synthesized arrays have the same angular resolution at high SNR values, for the low SNR range (10dB), the synthesized arrays provide up to 2° improvement in angular resolution over MRA-MIMO and about 8° over ULA-MIMO. Similarly, for 3Tx4Rx Synthesized MIMO the angular resolution has improved by 3° (twice) over ULA-MIMO at high SNR. And at the low-SNR range, the synthesized array provides an improvement of about 2° over MRA-MIMO and about 5° over ULA-MIMO.

The synthesized arrays have the advantage in a low-SNR environment. The sparse recovery algorithms BPDN and FOCUSS perform the best among the tested algorithms. BPDN works better in a low-SNR environment, and FOCUSS performs better in high-SNR applications. And both of the algorithms have the same level of complexity. The selection of the algorithm will depend on the application and the noise in the system. Hence, the synthesized arrays combined with one of these algorithms should provide optimal performance.

5.2. FUTURE WORK

1. Further optimization of the proposed algorithm can be investigated. The proposed algorithm is sensitive to different starting array element positions, investigation needs to be done to find the optimal starting point.
2. The extensions (Section 3.5) provided in the thesis are for linear array (SIMO), they need to be developed for MIMO configurations as well.
3. A technique to implement automatic norm minimization algorithm for non-uniform sparse MIMO should be developed to avoid the grid-mismatch problems in DOA estimation.
4. The sparse recovery algorithms have been tested for single and dual targets. Multi-target analysis and shortcomings need to be investigated further.

REFERENCES

- [1] S. M. Patole, M. Torlak, D. Wang, and M. Ali, "Automotive radars: A review of signal processing techniques," *IEEE Signal Processing Magazine*, vol. 34, no. 2, pp. 22–35, 2017.
- [2] D. Rabideau and P. Parker, "Ubiquitous mimo multifunction digital array radar," in *The Thrity-Seventh Asilomar Conference on Signals, Systems Computers, 2003*, vol. 1, pp. 1057–1064 Vol.1, 2003.
- [3] A. M. Haimovich, R. S. Blum, and L. J. Cimini, "Mimo radar with widely separated antennas," *IEEE Signal Processing Magazine*, vol. 25, no. 1, pp. 116–129, 2008.
- [4] J. Li and P. Stoica, "Mimo radar with colocated antennas," *IEEE Signal Processing Magazine*, vol. 24, no. 5, pp. 106–114, 2007.
- [5] M. Rani, S. B. Dhok, and R. B. Deshmukh, "A systematic review of compressive sensing: Concepts, implementations and applications," *IEEE Access*, vol. 6, pp. 4875–4894, 2018.
- [6] R. Baraniuk, M. A. Davenport, M. F. Duarte, C. Hegde, *et al.*, "An introduction to compressive sensing," *Connexions e-textbook*, pp. 24–76, 2011.
- [7] E. J. Candès, "The restricted isometry property and its implications for compressed sensing," *Comptes Rendus Mathematique*, vol. 346, no. 9, pp. 589–592, 2008.
- [8] E. Candes and J. Romberg, "Sparsity and incoherence in compressive sampling," *Inverse problems*, vol. 23, no. 3, p. 969, 2007.
- [9] A. Moffet, "Minimum-redundancy linear arrays," *IEEE Transactions on antennas and propagation*, vol. 16, no. 2, pp. 172–175, 1968.
- [10] C.-Y. Chen and P. P. Vaidyanathan, "Minimum redundancy mimo radars," in *2008 IEEE International Symposium on Circuits and Systems*, pp. 45–48, 2008.
- [11] D. Kurup, M. Himdi, and A. Rydberg, "Synthesis of uniform amplitude unequally spaced antenna arrays using the differential evolution algorithm," *IEEE Transactions on Antennas and Propagation*, vol. 51, no. 9, pp. 2210–2217, 2003.
- [12] M. Ridwan, M. Abdo, and E. Jorswieck, "Design of non-uniform antenna arrays using genetic algorithm," in *13th International Conference on Advanced Communication Technology (ICACT2011)*, pp. 422–427, 2011.
- [13] H. Oraizi and M. Fallahpour, "Nonuniformly spaced linear array design for the specified beamwidth/sidelobe level or specified directivity/sidelobe level with coupling consideration," *Progress In Electromagnetics Research*, vol. 4, pp. 185–209, 2008.
- [14] N. Jin and Y. Rahmat-Samii, "Advances in particle swarm optimization for antenna designs: Real-number, binary, single-objective and multiobjective implementations," *IEEE Transactions on Antennas and Propagation*, vol. 55, no. 3, pp. 556–567, 2007.

- [15] M. Skolnik, R. Collin, and F. Zucker, "Nonuniform arrays in antenna theory," in *Part I*, p. 19, McGraw-Hill, 1969.
- [16] O. M. Bucci, M. D'Urso, T. Isernia, P. Angeletti, and G. Toso, "Deterministic synthesis of uniform amplitude sparse arrays via new density taper techniques," *IEEE Transactions on Antennas and Propagation*, vol. 58, no. 6, pp. 1949–1958, 2010.
- [17] M. Viganó and D. Caratelli, "Analytical synthesis technique for uniform-amplitude linear sparse arrays," in *2010 IEEE Antennas and Propagation Society International Symposium*, pp. 1–4, IEEE, 2010.
- [18] A. F. Morabito, T. Isernia, and L. Di Donato, "Optimal synthesis of phase-only reconfigurable linear sparse arrays having uniform-amplitude excitations," *Progress In Electromagnetics Research*, vol. 124, pp. 405–423, 2012.
- [19] H. Lebrecht and S. Boyd, "Antenna array pattern synthesis via convex optimization," *IEEE Transactions on Signal Processing*, vol. 45, no. 3, pp. 526–532, 1997.
- [20] S. E. Nai, W. Ser, Z. L. Yu, and H. Chen, "Beampattern synthesis for linear and planar arrays with antenna selection by convex optimization," *IEEE Transactions on Antennas and Propagation*, vol. 58, no. 12, pp. 3923–3930, 2010.
- [21] G. Prisco and M. D'Urso, "Maximally sparse arrays via sequential convex optimizations," *IEEE Antennas and Wireless Propagation Letters*, vol. 11, pp. 192–195, 2012.
- [22] C. Bencivenni, M. Ivashina, R. Maaskant, and J. Wettergren, "Design of maximally sparse antenna arrays in the presence of mutual coupling," *IEEE Antennas and Wireless Propagation Letters*, vol. 14, pp. 159–162, 2014.
- [23] Y. Aslan, J. Puskely, A. Roederer, and A. Yarovoy, "Synthesis of multiple beam linear arrays with uniform amplitudes," in *12th European Conference on Antennas and Propagation (EuCAP 2018)*, pp. 1–5, 2018.
- [24] D. L. Donoho, X. Huo, *et al.*, "Uncertainty principles and ideal atomic decomposition," *IEEE transactions on information theory*, vol. 47, no. 7, pp. 2845–2862, 2001.
- [25] Z. Ben-Haim, Y. C. Eldar, and M. Elad, "Coherence-based performance guarantees for estimating a sparse vector under random noise," *IEEE Transactions on Signal Processing*, vol. 58, no. 10, pp. 5030–5043, 2010.
- [26] M. H. Agha, M. A. Al-Adwany, O. Bayat, and H. T. Hamdoon, "Optimization of antenna array pattern for uniformly excited rectangular array via thinning," *Journal of King Saud University-Engineering Sciences*, 2021.
- [27] G. Toso, P. Angeletti, and C. Mangenot, "A comparison of density and amplitude tapering for transmit active arrays," in *2009 3rd European Conference on Antennas and Propagation*, pp. 840–843, 2009.
- [28] B. Fuchs, A. Skrivervik, and J. R. Mosig, "Synthesis of uniform amplitude focused beam arrays," *IEEE Antennas and Wireless Propagation Letters*, vol. 11, pp. 1178–1181, 2012.

- [29] R. Haupt, "Thinned arrays using genetic algorithms," *IEEE Transactions on Antennas and Propagation*, vol. 42, no. 7, pp. 993–999, 1994.
- [30] L. Cen, Z. L. Yu, W. Ser, and W. Cen, "Linear aperiodic array synthesis using an improved genetic algorithm," *IEEE Transactions on Antennas and Propagation*, vol. 60, no. 2, pp. 895–902, 2011.
- [31] Y. Aslan, J. Puskely, A. Roederer, and A. Yarovoy, "Multiple beam synthesis of passively cooled 5g planar arrays using convex optimization," *IEEE Transactions on Antennas and Propagation*, vol. 68, no. 5, pp. 3557–3566, 2020.
- [32] M. S. Lobo, L. Vandenberghe, S. Boyd, and H. Lebert, "Applications of second-order cone programming," *Linear algebra and its applications*, vol. 284, no. 1-3, pp. 193–228, 1998.
- [33] M. Grant and S. Boyd, "CVX: Matlab software for disciplined convex programming, version 2.1." <http://cvxr.com/cvx>, Mar. 2014.
- [34] S. Kirkpatrick, C. D. Gelatt, and M. P. Vecchi, "Optimization by simulated annealing," *science*, vol. 220, no. 4598, pp. 671–680, 1983.
- [35] J. A. Tropp and S. J. Wright, "Computational methods for sparse solution of linear inverse problems," *Proceedings of the IEEE*, vol. 98, no. 6, pp. 948–958, 2010.
- [36] G. Cormode, "Sketch techniques for approximate query processing," *Foundations and Trends in Databases. NOW publishers*, 2011.
- [37] S. Ji and L. Carin, "Bayesian compressive sensing and projection optimization," in *Proceedings of the 24th international conference on Machine learning*, pp. 377–384, 2007.
- [38] S. S. Chen, D. L. Donoho, and M. A. Saunders, "Atomic decomposition by basis pursuit," *SIAM review*, vol. 43, no. 1, pp. 129–159, 2001.
- [39] R. Tibshirani, "Regression shrinkage and selection via the lasso," *Journal of the Royal Statistical Society: Series B (Methodological)*, vol. 58, no. 1, pp. 267–288, 1996.
- [40] Y. C. Pati, R. Rezaifar, and P. S. Krishnaprasad, "Orthogonal matching pursuit: Recursive function approximation with applications to wavelet decomposition," in *Proceedings of 27th Asilomar conference on signals, systems and computers*, pp. 40–44, IEEE, 1993.
- [41] D. Needell and J. A. Tropp, "Cosamp: Iterative signal recovery from incomplete and inaccurate samples," *Applied and computational harmonic analysis*, vol. 26, no. 3, pp. 301–321, 2009.
- [42] T. Blumensath and M. E. Davies, "Normalized iterative hard thresholding: Guaranteed stability and performance," *IEEE Journal of selected topics in signal processing*, vol. 4, no. 2, pp. 298–309, 2010.

- [43] I. F. Gorodnitsky and B. D. Rao, "Sparse signal reconstruction from limited data using focuss: A re-weighted minimum norm algorithm," *IEEE Transactions on signal processing*, vol. 45, no. 3, pp. 600–616, 1997.
- [44] B. D. Rao, K. Engan, S. F. Cotter, J. Palmer, and K. Kreutz-Delgado, "Subset selection in noise based on diversity measure minimization," *IEEE transactions on Signal processing*, vol. 51, no. 3, pp. 760–770, 2003.
- [45] B. Lin, J. Liu, M. Xie, and J. Zhu, "Super-resolution doa estimation using single snapshot via compressed sensing off the grid," in *2014 IEEE International Conference on Signal Processing, Communications and Computing (ICSPCC)*, pp. 825–829, 2014.
- [46] Z. Yang, J. Li, P. Stoica, and L. Xie, "Sparse methods for direction-of-arrival estimation," in *Academic Press Library in Signal Processing, Volume 7*, pp. 509–581, Elsevier, 2018.
- [47] H. Chung, J. Joo, and S. Kim, "Off-grid doa estimation on non-uniform linear array using constrained hermitian matrix," *Energies*, vol. 13, no. 21, p. 5775, 2020.
- [48] M. Wagner, Y. Park, and P. Gerstoft, "Gridless doa estimation and root-music for non-uniform linear arrays," *IEEE Transactions on Signal Processing*, vol. 69, pp. 2144–2157, 2021.
- [49] Q. Ren and A. Willis, "Extending music to single snapshot and on line direction finding applications," 1997.
- [50] W. Liao and A. Fannjiang, "Music for single-snapshot spectral estimation: Stability and super-resolution," *Applied and Computational Harmonic Analysis*, vol. 40, no. 1, pp. 33–67, 2016.
- [51] A. Hassanien, M. G. Amin, Y. D. Zhang, and F. Ahmad, "High-resolution single-snapshot doa estimation in mimo radar with colocated antennas," in *2015 IEEE Radar Conference (RadarCon)*, pp. 1134–1138, IEEE, 2015.
- [52] C. Degen, "On single snapshot direction-of-arrival estimation," in *2017 IEEE International Conference on Wireless for Space and Extreme Environments (WiSEE)*, pp. 92–97, IEEE, 2017.
- [53] P. Stoica and K. Sharman, "Maximum likelihood methods for direction-of-arrival estimation," *IEEE Transactions on Acoustics, Speech, and Signal Processing*, vol. 38, no. 7, pp. 1132–1143, 1990.
- [54] I. Ziskind and M. Wax, "Maximum likelihood localization of multiple sources by alternating projection," *IEEE Transactions on Acoustics, Speech, and Signal Processing*, vol. 36, no. 10, pp. 1553–1560, 1988.